Integrated data analysis: ST2, CB1 and ST1

Simran Johal

Supervisor: Raymi Castilla

Contents

1. Introduction

Six long boreholes (~ 200 - 400m) have been drilled at the Bedretto Underground Laboratory for Geoenergies (BULG). The data collected on these 6 boreholes is abundant. Drilling logs, cores, wireline logs, videos, hydraulic tests and Ground Penetrating Radar (GPR) are some of the datasets available to build a coherent model. So far, these data have been used in isolation to build partial pictures of the BULG (Structural interpretation, hydraulic characterisation, etc) and a comprehensive analysis is still lacking.

The main objective of this project is to build an integrated view of the main features identified in different datasets. Through this integrated analysis we will pinpoint the different responses that different important features show in different datasets. Some of the main questions that will be answered are: Do the main fault zones identified in the structural analysis correspond always to high inflow zones identified through hydraulic tests and strong reflectors in GPR images? Are these same features identifiable through the analysis of drilling data and rate of penetration (ROP) logs? The focus will first be on the ST1 and ST2 boreholes (specially ST2) and then to move on afterwards to the MB wells (MB1, MB2, MB3 and MB4).

Is there enough evidence to provide that boreholes ST2 and CB1 are sufficiently connected? The cementation of CB1 is a possible further step in the Bedretto lab testing, and it needs to be understood whether or not the cement particles will flood into ST2.

Therefore, the work outlined in the report hopes to find evidence to help understand the connectivity between ST2, ST1 and CB1 which will then impact further courses of action in the Bedretto tunnel and to help constrain drilling techniques.

2. Available Datasets

The data that was utilized in this analysis was mainly sources from experiments run from Late August to Early September 2020. All are property of GES, unless stated otherwise.

1. Optical Televiewer (OPTV) logs
2. ATV (Amplitude Televiewer Logs
3. Total Gamma Ray (GR) logs
4. Fracture Mapping Data- Raymi Castilla, GES
5. Spectral Gamma Ray Logs
6. Spinner Logs and derived flow meter logs
7. Temperature and Electrical Conductivity logs
8. Hydraulic test data with field logbook- Fabien Christe, Francisco Serbeto, Peter Meier, GES
9. Overall Bedretto structure 3D images, Raymi Castilla, GES
10. Ground Penetrating Radar (GPR) in boreholes
11. P-wave velocities **– Uni Löben- Andrew Greenwood & Eva Caspari**
12. P-wave stacking methods **– Uni Löben- Andrew Greenwood & Eva Caspari**
13. Drilling Data- Drilling Progress, Rotation Pressure, Circulation Pressure, Contact Pressure and Counter Pressure- **Florian Özkoral, Züblin Spezialtiefbau Ges.m.b.H.**
14. 2D borehole temperature imaging- **ETH Nima Gholizadeh**
15. Structural fracture interpretations through all the Bedretto Boreholes- Raymi Castilla, 2020

3. Methods

The Methods employed in this study involved direct analysis of data from the logs being put into a large Composite Log. Apart from analysis of the collected data, some addition data manipulation was carried out to be able to extract more interpretations / visualize the data more effectively.

3.1. Conversion to Flow meter data

The spinner data that was presented from the borehole tests provides data in terms of cycles per second, which is not a format of flow rates; that would be more suited for analysis. Therefore, by utilizing the fluid velocity and caliper data, it is possible to convert this to obtain a depth-running flow rate.

The data used was from the 20200807 flow up tests in ST2, where flow up was measured for a test where the spinner travelled down and the up again. The spinner data used in ST1 measured the flow down when the spinner was moving down, and the flow up when the spinner was moving up. Data interpolation and a calibration is also completed to reduce noise signals and align the data correctly.

Governing Equations

In the borehole upward fluid motion is taken as negative. Therefore, when the spinner is run in the opposite direction to the fluid velocity, the relative velocity will be larger than the logging velocity.

$$V_r = V_l - V_f \qquad (1)$$

Where, V_r = relative velocity [m/s] V_l = logging velocity [m/s] V_f = fluid velocity [m/s]

The calibration uses the logging speed plotted against the cycles per second (CPS) to correct the relative velocity values with depth. The effects of bearing friction, fluid density and viscosity on the impeller and geometry of the sonde are accounted for.

Calibration:

$$V_r(z) = (S(z) * C_{v-down}) + S_{o-down} \qquad (2)$$

$$V_r(z) = \left(S(z) * C_{v-up}\right) + S_{o-up} \qquad (3)$$

(z) = depth [m] $C_{v-up\ or\ down}$ = linear coefficient of log speed vs CPS $S_{o-up\ or\ down}$ = stall speed [m/s]

where there is no rotation with the sonde.

Thus,

$$V_f(z) = V_l - \left(S(z) * C_{v-up}\right) + S_{o-down} \qquad (4)$$

This allows the flow rate to be calculated:

$$Q(z) = V_f(z) * A(z) \qquad (5)$$

$Q(z)$ = Flow rate wrt. Depth [m^3/s] $A(z)$ = Area of the borehole wrt. Depth. [m^2]

The final plots are shown in the WellCAD composite logs.

Since no attempt was made to calibrate the spinner in the test boreholes, the calibration values required were taken from ETH Borehole Geophysics lecture by Prof. Dr. Hansruedi Maurer. These values provided more plausible results. The flow up spinner results run 4 were transformed into flow rates and velocity.

3.2. Hydraulic Interval Pressure-time graph ratios

In order to see the 'extent' of hydraulic influence between the Pressure time graphs of the boreholes, ratios were calculated to quantify this. The ratios were taken from 2 observation points: the packer deflation and the influence of opening a borehole (often it was the opening of CB1) and were [CB1_pressure/ST2_pressure]. This is illustrated in the figure below.

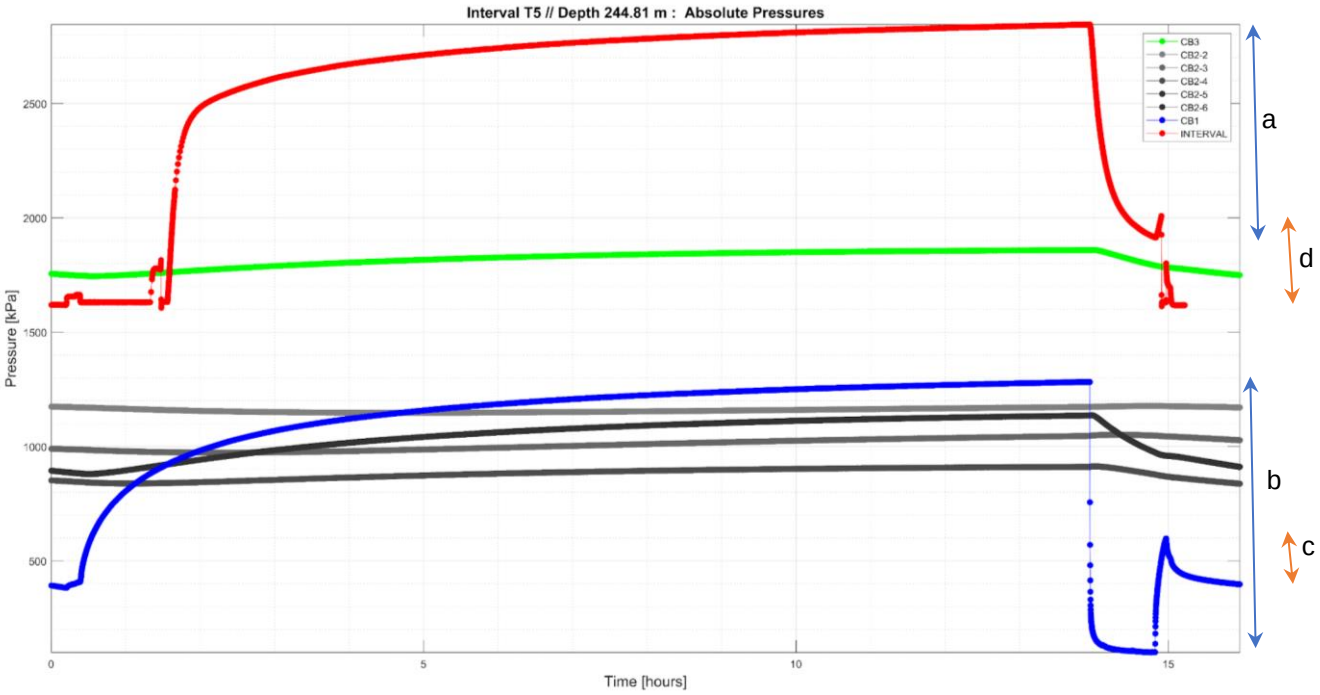

b/a = Ratio for Shut in valve opening c/d = Ratio for deflation of the packers

Ratios were made in an attempt to quantify the extent of response intensity.

3.3. Stereonets: Polar Geometric Data Plotting

WellCAD software has a function enabling the stereonet to be plotted based on the structures drawing on the logs. The correction from the High Side of the borehole (which the 3D log shows) to the Magnetic north direction is calculated by WellCAD. Then, the Magnetic North oriented data is used for plotting stereonets with pole contours and great circles.

For the boreholes ST2 and CB1, it is fitting to create stereonets at the locations of the intervals where the hydraulic tests were completed and where major fault zones are identified. In ST1, there have not currently been hydraulic tests where hydraulic intervals have been defined, therefore stereonets were taken at 40 m intervals.

3.4. Drilling Data Acquisition

Drilling of the ST2 and ST1 boreholes was carried out by Züblin Spezialtiefbau G.m.b.h and data was obtained on the Rotation Pressure, Rotation Speed, Circulation Pressure, Drilling Speed, Counter Pressure, Contact Pressure, Drilling Progress, Jet Pressure and Jet Flow. A drilling hammer was used and thus the borehole was drilled via percussion drilling.

Figure 1- Images showing the drilling hammer with the drill hammer bit. There are 3 holes that allow for the drilling mud to be transferred up the drill string.

A few comments of the Drilling Process that are relevant to the data analysis are as follows:

- When the Drill Bits were changed, the same models were used to continue drilling.
- ST1 Drill bit changes locations: 64 m, 122 m, 261m and 351 m.
- ST2 Drill bit changes locations: 138 m, 207 m and 306 m.
- Water Jet inflow was measured using an Inductive flow meter, but is not considered in the results and discussion as this is purely to do with the drilling process and not in relation to the formation.
- Rotation Pressure and Rotation Speed are different and they do not change with the lithology conditions, thus they are also not considered.

Contact and Counter Pressure

Counter pressure is applied by the drill rig to tension the drill string and to hold it up to prevent buckling from occurring.

The Contact pressure is the weight on the bit, whenever the bit comes into contact with the bottom of the borehole.

Drilling Progress and Drilling Speed

Drilling Progress describes the rate of progressing of the drill bit through the formation, in units of m/hr measured by the sensors on the drill rig.

The Drill speed was not provided by Züblin, hence was calculated from the existing time and depth interval data. Where a simple depth divided by time calculation was computed. The resulting Drilling Speed patterns for both ST1 and ST2 followed the same trend as the Drilling Progress, in units m/min.

3.5. Fracture connecting

This was done by identifying larger zones of fractures/faults and comparing the spatial depths within each borehole to find fractures that match. Analysis of the OTV and ATV logs allows the correlation of fractures based on the fracture thickness, depth and relative positioning. The connections are named using the system provided by R. Castilla, 2020, and follow the overall trend in the diagram below. Any additional fracture features are given another label and specified.

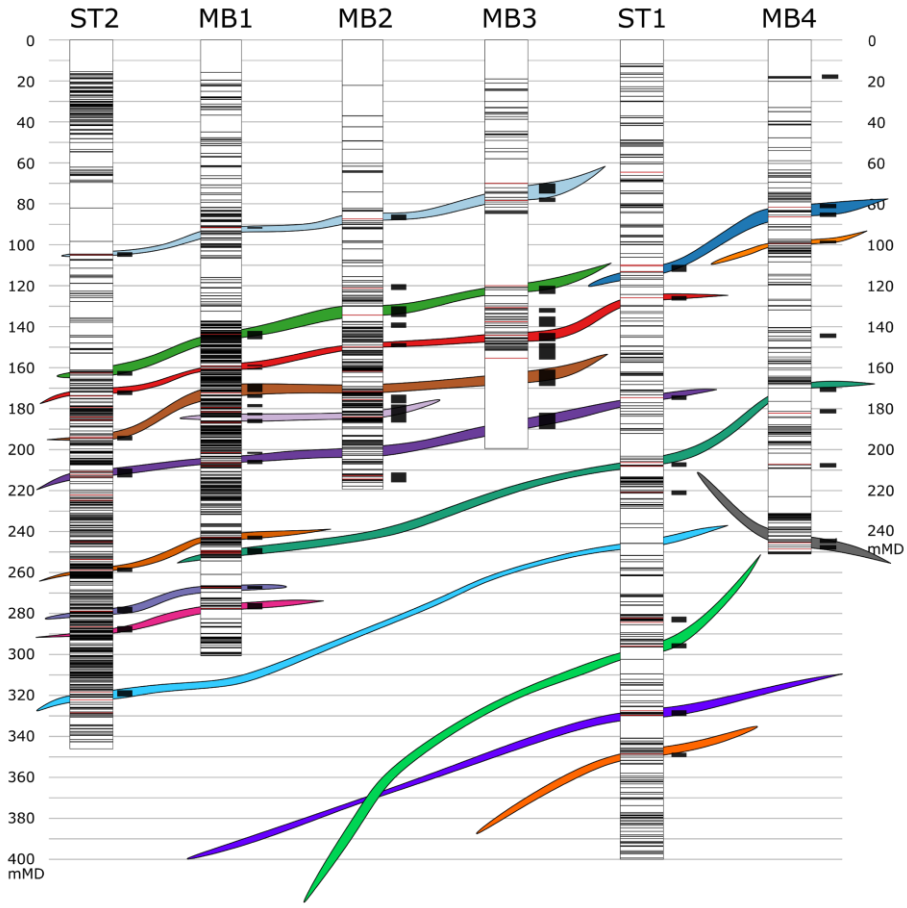

Figure 2- Fracture connections based on Structural data, proposed by R. Castilla, 2020

The process involved using a mix of Geophysical data and Drilling data, with the results discussed in section 4.1.1.

3.6. P-wave velocity and semblance stacking

When considering P-waves with respect to fractures, there are 2 available data sets to work with P-wave velocity and P-wave semblance stacking.

The P-wave semblance stacking analysis is carried out by reading where the stacks reach values at the mid-level of the scale, at 500 micro seconds (µs) for the cases of ST1 and ST2. In these intervals larger (interference) zones of 500 µs are related to larger fracture zones. The interference zones were qualitatively put into categories based on their strength, shown in table 2. Higher strength zones were observed when the 500 µs areas penetrate the whole stack.

The P wave velocity is plotted against depth and is given as a simple graph, whereby reductions in velocity can be observed.

4. Results and Discussions

4.1- Structural Analysis

4.1.1. Fracture Connections: ST2, CB1 and ST1

Table 1 below summarizes the results of the Fracture connection analysis. There are columns for the depth and whether the observed fracture connection falls into a hydraulic interval for the case of ST2 and CB1. So, for each fracture in ST2 and CB1 there is not necessarily a hydraulic interval stated for everyone. In most cases connections between fractures in ST2 and CB1, were roughly 10m vertically apart (CB1 fractures at a lower measured depth), whereas the fractures between ST1 and ST2 vary by around 50 m in measured depth for the top of the boreholes, figure 2.

Note: Spike in the table below refers to a Drilling Progress peak.

Official Fault Name **ID**	Connection	Interval / Depth			ST2	P wave	CB1	ST1	P wave
		ST2	CB1	ST1					
No reference	**1.1***	T9 302 m	289.5 m		Individual fracture, Eastward dip 80 uS/cm Spike 50 m/h		Individual fracture, no eastward dip 100 uS/m		
15 st2_286	**1***	T8 287m	HT 12 277.5 m		Fault Zone, 0.5 m, vertical 89.7° Electrical Cond. Increase 50 uS/cm Spike 50 m/h Many stereonet orientations		Fault Zone, 0.4 m Electrical Cond. Increase 100 uS/cm		
13 st2_278	**2***	T7 279 m	HT 11 267 m		Fault Zone, 0.5 m Noise on EC Spike 40 m/h		Fault Zone, 0.9 m Noise on EC		
11 St2_258	**3***	T6 259 m	HT 10 250 m	221 m	Fault Zone, 0.75 m Spike 40 m/h		3 Fault Zones, 1.5 m	Fault Zone, 0.3 m 2 Spikes 30 m/h 1 plane east	
No reference	**4***	T5 254 m	HT9 243 m	207 – 209 m	Fault Zone, 2 m No clear spike		Fault Zone, 0.75 m	2 fault zones, 0.25 m and 0.3 m Wide spike 30 m/h	
No reference	**3***	T5 253 m	HT9 241 m		Fracture plane dipping East-Irregular No drill spike	None	Fracture plane dipping East-Irregular		
No reference	**4***	T5 245 m	HT8 236 m		Fault Zone, 2 m No drill spike	No	Similar faults seen based on spacing, but not classed as a fault zone.		
No reference	**5***	T4 225 m	HT 5 208 m	175 m	Fault Zone, 1.2 m Spike 40 m/h		Fault Zone, 0.75 m	Fault Zone, 0.2 m Spike 40 m/h	
No reference	**6***	T4 222.5 m	HT5 206 m	171 m	Thin fault zone Spike 30 m/h		Fault Zone, 0.7 m	Marked as a fracture- possibly could be a fracture zone No spike~30 m/h	

10 St2_213	**7***	T3 213 m	201 m		2 Fault Zones, 2 m Spike 70 m/h		Fault Zone, 0.7 m		
10 St2_210	**8***	T3 210.5 m	HT 4 198 m		2 defined fractures, 0.5 m apart Spike 50 m/h (above is a high zone 100 m/h)		1 Fault Zone, 0.5 m ATV looks like 2 fractures		
8 St2_193	**9***	F2a 194 m	HT3 186 m	146 m	2 fault zones, 1.5 m Spike 40 m/h		Fault Zones, 1 m	Possible Fault Structure No spike	
No reference	**10***	F1 186 m	HT2 181.5 m	142 m	Fault Zone, 0.8 m Spike 60 m/h		Fault Zone, 0.6 m Gamma Peak	Fault Zone, 0.5 m Spike 40 m/h	
No reference	**11***	F1 184 m	HT2 179 m	140 m	Fault Zone, 1.2 m Spike 30 m/h		Fault Zone, 1.5 m Gamma Peak	2 individual fractures with 0.25 m width. No spike	
7 St2_179	**12***	F1 179 m	172 m	130 m	Fault Zone, 1 m Spike 70 m/h		Fault Zone, 1.2 m	Peak in Gamma Group of fractures, 0.5 m Spike 40 m/h	
7 St2_173	**5***	T2 174 m	160 m	126 m	Temp and EC increase downhole High transmissivity Fault Zone, 0.2 m Spike 75 m/h		2 Fault Zones, both 0.6 m	Fault Zone, 0.75 m Spike 30 m/h	
2 St2_162	**6***	T1 162 162.5 m	HT 1 144 m	106 – 114 m	Fault Zone, 2 m Spike large wide 60-70 m/h		Fault Zone, 1.2 m	Downhole drop in temp and conductivity Fault Zone, 6 m Wide Spike ~60 m/h	

Table 1- Proposed fracture connections labelled from ST1, ST2 and CB1 integrated with P-wave data and drilling data included.

For 'Connection' column: Purple= more sure, Orange = less sure

P wave signal		
Strong		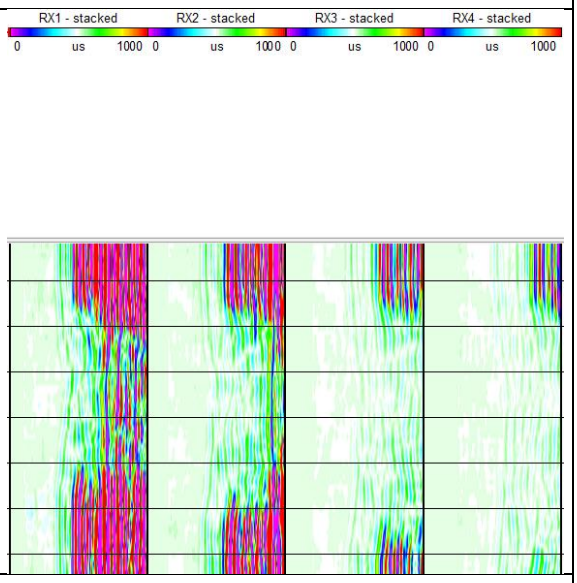
Medium		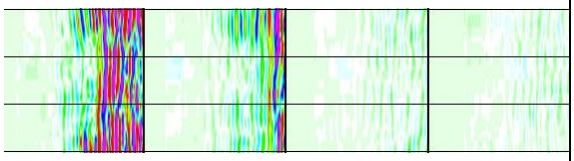
Weak		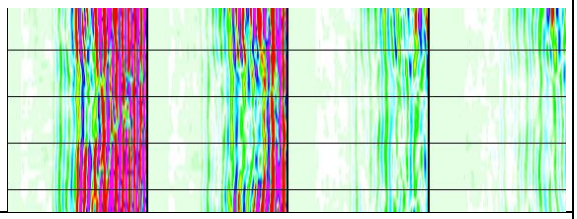
Very Weak		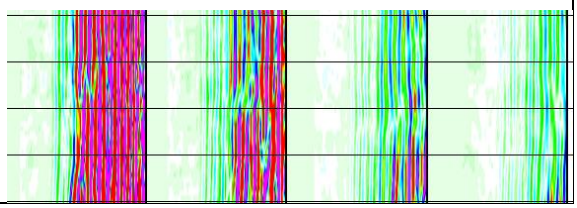

Table 2- P-wave signal stack qualitative analysis interference levels with images from the logging.

Naming of the Fault Zones

The official fault zone naming was carried out by R. Castilla, and have been associated with corresponding structural connections, Figure 2. The 'connection' column in Table 1, were the proposed connections that made during this study were based on spatially comparing the locations of fractures mainly in ST2 and CB1. Wherever there is no reference to the official fault zone names, the connection names are used.

Interpretation

From this analysis, it was found that fault zones that experienced spikes in Drilling Progress, also portrayed P-wave signals. The few connections proposed that did not involve fault zones, e.g. **3*** and **4*** did not show any Drilling Progress spikes or P wave signals, therefore the surety of this connection is comprised and thus can be considered to be not a real connection. In general, if a P wave signal was strong in one fault zone, then it tended to be strong in the others, e.g. ST2_162 and ST2_179. Similar trends were seen in the weak P-wave zones, e.g. **6*** and **11***. However, these trends are weak and do not apply to all fracture zones.

When considering the Drilling Progress spikes, the magnitudes varied in between the boreholes, and therefore could not be used as a feature to identify a fault zone between boreholes. This was expected, as over 10s of meters a fault zone can vary in fault core thickness, amount of fault gouge etc. Therefore, the drilling progress spikes only inform of the presence of a fault down the borehole that data has been collected for.

4.1.2. Structural Orientations through Stereonet analysis

The respective stereonets for Tables 3 and 4 are plotted in the WellCAD files included as part of Appendix E, F and G. The tables below summarize the important observations from the stereonets for each borehole.

ST2

Interval	**Mean Dip Direction°/Dip° /+ major fault orientations**	**Change from previous Interval + notable observations**
T1	328/57	-
T2	339/60	-
F1	336/53	Higher fracture density
F2a	339/63	Here there is one fault zone-oriented NW-SE, which is different to all other fault zones
T3	331/ 65	-
T4	328/ 63	-
T5	315/57	-
T6	333/56	High fracture density
T7	070/33	Suddenly more variable orientation where we have 2 fracture orientations. Poles plot in the SW corner whereas before they continuously plotted in the SE.
T8	000/76 2 orientations: 340/66 and 230/80	Interval with highest fracture density. There is a E-W completely **vertical fault zone** present here.
T9	304/78 2 orientations: 310/80 and 034/80	Shows similar to T8- 2 main sets.
T10	349/69 2 orientations: 020/80 and 350/70	Moving towards the SE pole direction of T6 again. Fractures here are oriented more E-W than all the other zones.
T12	318/68	Pole direction now firmly SE.

Table 3- ST2 Stereonet orientation analysis taken from structures within the hydraulic test intervals, with Dip Direction/Dip data and any changes from the previous interval noted.

CB1

Interval	**Mean Dip Direction°/Dip° /+ major fault orientations**	**Change from previous interval**
HT-1	338/57	- Poles plot SE
HT-2	344/53	Planes become more East-West orientated
HT-3	343/45	Not much change, overlap with HT-2
HT-4	345/46	-
HT-5	334/63	Planes plot more north east
HT-6	339/68	A few (3) N-S planes all dipping towards the west present.
HT-7	332/60	Planes oriented more NE-SW, N-S orientation gone. Beginning to see NW-SE oriented planes. No fault zones present.

HT-8	205/69	2 discrete plane orientations. More planes oriented NW-SE rather than the larger preferred plane. Therefore, the stereonet poles plot in the NE corner.
HT-9	359/72	There is a fault zone present that still plots 338/74 Consistently steeper dip for all orientations. Much more variability in the orientations, still the NE-SW and NW-SE planes can be identified as sets. 2 pole regions identified.
HT-10	340/61	Return to the NE-SW direction, poles plot in SE corner. There is only one plane oriented NW-SE.
HT-11	339/73	Less variability, captures a zone which has faults but also smaller fractures within it too. NE-SW orientation
HT-12	331/76 2 orientations: 136/88 339/50	Both planes strike NE-SW, however one set dips to the NW (which is usual) and the other dis to the SE which is unusual. There are only 4 planes that do this however, thus it may require more investigation.

Table 4- CB1 Stereonet orientation analysis taken from structures within the hydraulic test intervals, with Dip Direction/ Dip data and any changes from the previous interval noted.

ST1

Depth	**Mean Dip Direction° / Dip° + major fault orientations**	**Change from previous interval**
10 – 50 m	256/78	- Pole lies in the N-E quadrant NW-SE dip which is relatively shallow, compared to what is seen in the Rotondo Granite in general.
50- 90 m	313/67 3 orientations present Major orientation with fault zone associated: 331/68	The major plane orientation changes to more N-S with a steep dip.
90 – 130 m	308/70 Fault orientation: 331/64	The E-W structure orientation is not present anymore
130-170 m	326/57 Fault zone: 326/63	There is one main strike orientation N – S to NW-SE, but with largely varying dip directions.
170 – 210 m	328/55	High dip angles, dip direction still varies between E and W
210 – 250 m	325/55	-
250 – 290 m	320/58	-
290 – 330 m	03/88	Strike is mainly NE-SW. Presence of almost **vertical structures oriented N-S**
330 – 370 m	001/75	More variability in structures than before. Majority of the orientations strike NE-SW. 2 orientations present
370 – 410 m	344/66 3 orientations Fault orientation: 012/73	Very different from previous, one N-S orientation, another NE-SW and the other NW-SE. The N-S orientation is very steeply dipping.

Table 5- ST1 Stereonet orientation analysis taken from structures within the hydraulic test intervals, with Dip Direction/ Dip data and any changes from the previous interval noted.

Interpretations

From the stereonet intervals, the area between T6-T9 is interesting due to the change in orientation of the strike direction for NE-SW to NW-SE, figure 3. This change in orientation is only seen in the individual fractures, rather than the fault zones. Unfortunately, this is not clearly seen in the structures of CB1, however it is likely to be present in other data, worked on by R. Castilla, 2020. Is it possible that the fractures from the change in

orientations are responsible for the increased flow rates? This is to do with hydraulic testing of the intervals in ST2, which is reviewed in Section 4.2.

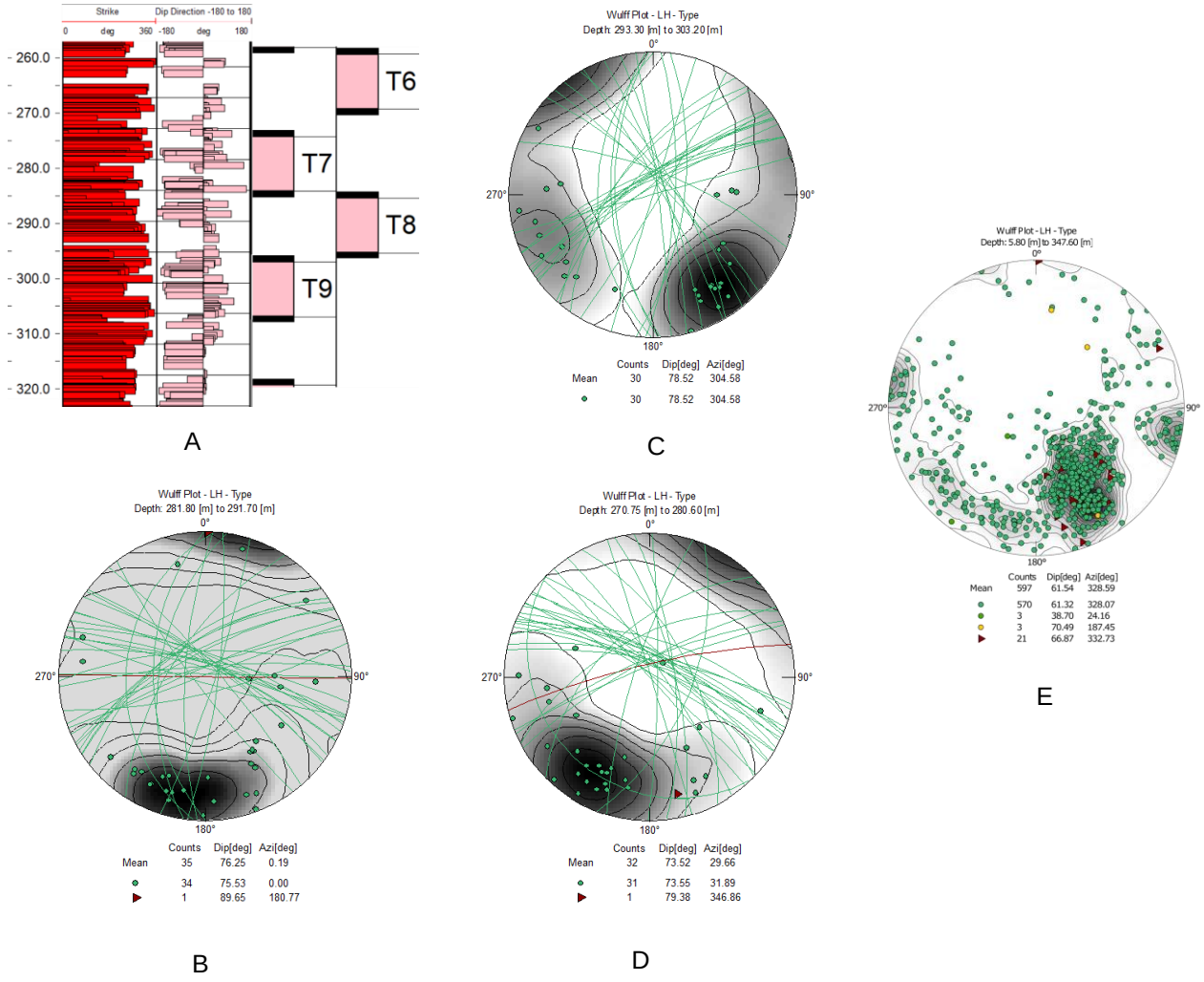

Figure 3- A) Bar representation of Strike and Dip direction through the intervals T6 – T9, B) Structure Stereonet interval T8 C) Structure Stereonet interval T7 D) Structure Stereonet interval T9 E) Structure Stereonet of whole borehole section. The 3 stereonets display 2 major orientations, one which is NW-SE that corresponds to what is seen in A. Green structures= individual fracture planes, Red structures= fault zones

The fact that there is a vertical fault zone present in T8 (Figure 3B), which was the highest flow interval suggests that vertical pathways may be the favorable for water to flow through the most. This occurs in conjunction with the dips of the planes in both ST2 and CB1 are becoming steeper down the borehole. An element of this can be attributed to depth, as the boreholes are drilled downwards with respect to the overall environment, which would require further 3D knowledge/ models. **The change in dip angle to more steep exists only over 180 m in a large Granitic mass,** which could be a geological inconsistency, but in any case, can inform us about the stress conditions of the rock. This is illustrated by the stereonets present in Figure 4.

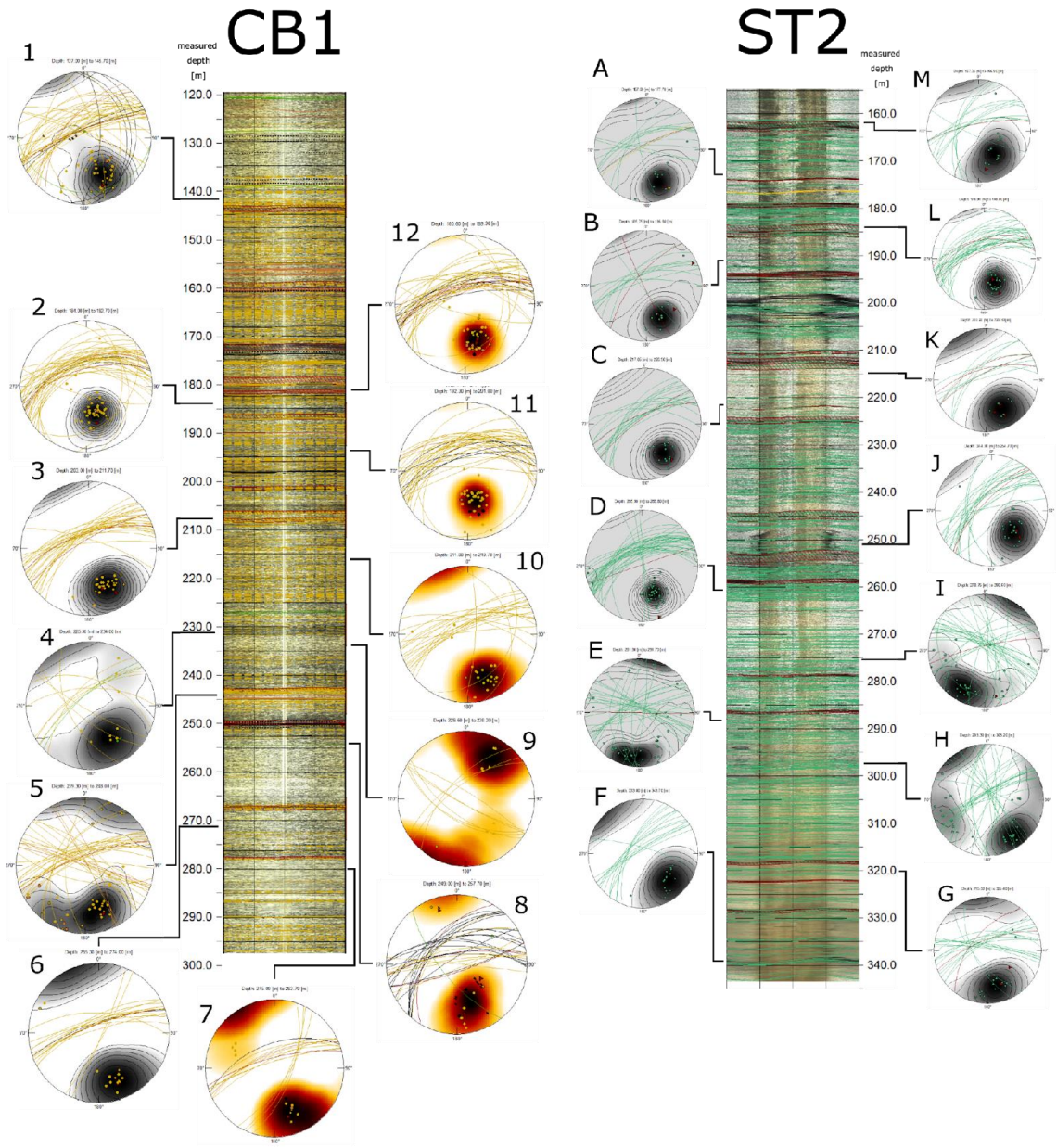

Figure 4- Boreholes CB1 and ST2 with the respective stereonets plotted from structural data in the hydraulic intervals. The respective depths are given for each stereonet in measured depth [m]: 1- 137 – 145, 2- 184 – 193, 3- 203 – 211, 4- 225 – 234, 5- 239 – 248, 6- 265 – 274, 7- 275 – 283, 8- 249 – 257, 9- 230 – 238, 10- 211 – 220, 11- 192 – 201, 12- 180 – 189, A- 167 – 177, B- 186 – 196, C- 217 – 227, D – 256 – 265, E- 262 – 292, F- 334 – 344, G- 316 – 325, H- 293 – 303, I- 271 – 281, J- 245 – 255, K- 210 – 220, L- 179 – 189, M- 157 - 167

The questions posed by this:

- How does the geology change through the overall structure of the Rotondo Granite?
- Are such 150 m scale changes of any significance?

In ST1, there is much more variation in the dip directions of the structures across the well. From the very beginning there are East dipping structures present as well as West. At the end of the borehole, the majority of the structure orientations are NW-SE and dip to the East more. This connects with the structures seen in ST2, T8 to T10 and possibly related to large water inflows in these intervals.

4.1.3. ST1 & ST2 Drilling Data Analysis

The Drilling data experiences an anomaly from 206 m to 210m, which affects every log in ST2.

Drilling Progress Observations

ST2:

- At 160 m, large spikes in Drilling Progress are observed until 220 m. This matches with the ATV images and OTV images which show high fracture density in the region.
- In ST2 it is known that before ca. 160 m measured depth, there is less fractured zone. Here the drilling progress is consistently around 15 m/hr.=-=
- After the zone at 220 m, the Drilling progress reduces to an average of 20 m/hr, which is larger than the drilling progress before. Despite still increasing amounts of fractures after 220 m. However, these structures do not create as large disturbances in the ATV images.
- This is more to do with the type of fractures present.
- Are the various spikes in Drilling Progress associated with the fault zones.
- It appears that the drill bit change at 207 m, has caused noise in the Drilling Progress and Drilling Speed therefore this is ignored.

ST1:

- From 10 – 65 m depth, the drilling progress spikes often, however, fracture density is not great here.
- From 65 – 105 m, the drilling progress reduces to an average of 10 m/hr.
- From 105 – 140 m, there are large spikes in drilling progress, which correlate to large fault zones seen in the OTV and ATV images.
- From 140 – 235 m, there are no large spikes and the average drilling progress is 20 m/hr, despite there still being fault zones present in this interval, though not as large as the ones before.
- From 235 – 345 m, there are more spikes and a higher average drilling rate of ca. 25 m/hr. This also includes a part from 235 – 275 m where little fractures are seen on the ATV and OTV.

ST2 Counter and Contact pressure observations

ST2:

- Counter pressure is increasing with depth, beginning at 20 bars, peaking at 170 bars at 330 m and then reducing to ~130 bars at the end 340 m.
- The Contact pressure is mainly at 50 bars, towards the end it is variable, dropping from 75 bars to 50 bars.

ST1:

- Counter pressure is increasing down the borehole.
- Contact pressure is stable at 55 bars**.** At 260 m, the counter pressure is significantly lower at 30 bars and increases 40 bars at 375 m. At 375 there is another drop in contact pressure, to 15 bars where it stays till the end.

Jet Flow and Pressure Observations

ST2:

- The Jet Flow stay constant for the most part, at 700 lt/min. It increases to 750 lt/min until 207 m, where there is a small drop back to 700 lt/min until 210 m. From there it increases to 750 lt/min.
- The Jet Pressure is slightly variable at the beginning but then stabilizes to 120 bars.

ST1:

- Jet flow is relatively stable at 560- 600 lt/min until 240 m where there is a sudden increase of 150 lt/min. After this the flow stay stable at 750 lt/min until the end.

- The Jet pressure is variable compared to the ST2 values. From 0 to 125 m the pressure is around 110 bars. From 125 m it is stable at 90 bars until 240 m where there is a sudden increase in pressure to 130 bars. At 350 m there is a reduction in pressure to 120 bars.

Interpretations

The jumps in the ST1 and ST2 Structures cumulative frequency chart correspond to larger spikes in Drilling Progress, in some cases. The jumps in Drilling progress are abrupt making it relatively easy to pinpoint them to a fault zone or section of fractures. See **Table 1 and Appendix D,** this is also discussed in conjunction to the P-wave data analysis in **Section 6.** For ST1 and ST2 the Drilling data confirms that drilling through the fracture zones result in higher Drilling progress rates as broken up rock and fault gouge has lower strength than the intact rock. (To further verify this then uniaxial test as well as using a Schmidt hammer would verify this).

In terms of the Contact pressures, the observations did not match well to the Drilling data or the Structural / Geophysical Data. Therefore, it can be concluded that this is related more or less only to the Drilling Process/ drill head parameters. The Counter Pressure however, shows a little correlation with the Drilling Progress in ST1, notably between 105 to 140 m in ST1 where there is a dip in counter pressure that relates to the interval of high Drilling Progress in ST1. This is seen at other where there are abrupt spikes in Drilling Progress in ST1. However, the Counter pressure drops do not relate to the fracture locations like the Drilling Progress, so it is not possible to use this data alone. The most it could be used for is verifying the quality of the drilling progress data. In ST2 the counter pressure does not closely follow the Drilling Progress, the most that was observed is a slight correlation in data noise at 180 m to 210 m, Appendices E and F.

The fact that in ST1 large spikes were observed that were not picked up by the ATV images but are present on the OTV suggest that the Drilling Progress is picking up individual fractures with spikes, but still only larger zones make clear spikes. It is also worth noting that in ST1 from 30 to 60 m depth, there is noise/spikes in the drilling progress, yet there are no significant larger fractures like in other regions. This reduces the accuracy of using drilling data, however, it may be a result just at the beginning of the borehole, as this is not seen to the same extent further down. This problem was not experienced in borehole ST2. Overall, it can be initially approximated that **60-80%** of the time the spikes in Drilling Progress can be associated to a fracture zone structures. This estimation would need to be confirmed with a numerical analysis.

4.2- Hydraulics Analysis

As part of the Hydraulic Reports on the Hydraulic tests completed by F. Christe, F. Serbeto and P. Meier, the following results were obtained:

For ST2, intervals T6, T5, F1a, T1a and T8 show the highest wellhead flow rates. The Transmissivity values considered were derived from the Jacob-Cooper solution of the first static pressure recovery test, and show that intervals T8, T2 and T3 are most transmissive. All the Transmissivity, Well head flow rate and interval location data for ST2 is included in **Appendix A**.

For CB1, intervals **HT-12, HT-3, and HT-9** show the highest wellhead flow rates. The transmissivity values considered were derived from the Jacob-Cooper solution of the first static pressure recovery test, and show that intervals HT-12, HT-3 and HT-2 are most transmissive. Within CB1, a positive correlation can be seen between the wellhead flow rate values and the transmissivity values. All the Transmissivity, Well head flow rate and interval location data for CB1 is included in **Appendix B**.

4.2.1. Hydraulic response between ST2 and CB1

The hydraulic relationship between the connectivity of ST2 and CB1 has been assessed by comparing the timings of the shut-in valve tests. Then it is possible to see the influence of hydraulic pressure changes in one borehole to another. Simplified visual representation of this influence:

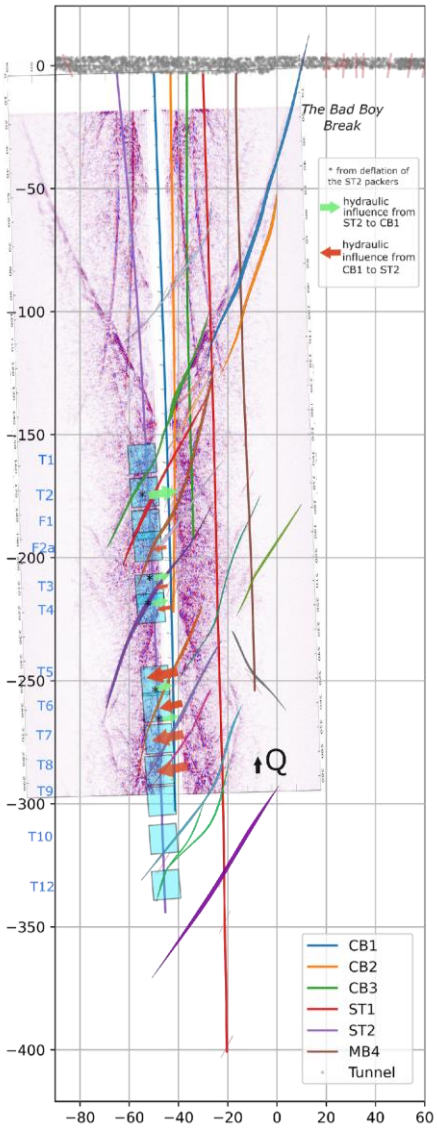

Figure 5- Diagram of the Bedretto boreholes, showing the hydraulic influence data visualized with arrows that reflect the ratio of the pressure changes between CB1 and ST2. This is overlayed on GPR images of fault structures predictions. Modified from R. Castilla, 2020.

Interval injection tests were carried out in ST2 and where CB1 is considered an observation borehole. The only changes made to CB1 were the shut ins of the boreholes, instead of the interval. (It makes sense that CB1 will exert greater influences on ST2 as you have changes in a within an interval vs changes in a borehole- but then again, the pressures in the interval are much higher in the intervals). The Hydraulic influences between the intervals reach larger extents at the zones T5 – T8.

- Within interval T5, a pressure drop of 900 kPa is witnessed with the opening of CB1 with a pressure drop of around 1200 kPa. (ratio 1.3)
- Within interval T6, a pressure drop of 400 kPa is witnessed with the opening of CB1 with a pressure drop of around 1000 kPa. (ratio 2.5)
- Within interval T7, a reaction from the closing of CB1 is first witnessed in ST2 here. CB1 pressure increase of 800 kPa results in a ST2 pressure increase of 600 kPa. (ratio 1.3)

- Within interval T8, a pressure drop of 350 kPa is witnessed with the opening of CB1 with a pressure drop of 450 kPa. (ratio 1.28)

The zones F2a to T4 show lesser extents of hydraulic connectivity with CB1, as pressure changes are on a much smaller scale:

- Within interval T4, a pressure drop of 20 kPa is witnessed with the opening of CB1 with a pressure drop of around 480 kPa. (ratio 24)

The intervals where a hydraulic influence was seen to be exerted from ST2 to CB1 were T2, T3, T4, T5, T6, where the deflation of the packers was present in the data frame. The only interval where it is known for sure that the deflation of the packers had no effect on CB1 was in interval F1.

Deflation Ratios:

- T2 ratio= 4
- T3 ratio = 0.4
- T4 ratio = 0.3
- T5 ratio = 0.5
- T6 ratio = 0.4

Large ratios (greater than 1) = more pressure influence from ST2 on to CB1 and vice versa.

Interpretations

From the ST2 and CB1 hydraulic test reports by F. Christe, F. Serbeto and P. Meier, it was concluded that the fractures connect hydraulically especially in the zones T5 to T8 where wellhead flow rates and transmissivities are higher. This is in accordance with what would be expected as higher transmissivities meaning that more water will flow through these fractures with time. From this further analysis with the hydraulic response ratios, Hydraulic 'Connectivity' between ST2 and CB1 increases further down the borehole of ST2 with CB1 exerting more hydraulic influence (pressure) from T5 to T8. This matches with the transmissivity and flow rate patterns.

Interval T2 is also highly transmissive, yet no changes in pressure of the interval when CB1 is opened. It is unclear why this happens. However, if the packer deflations are considered, this interval exerts a much larger influence on CB1 than the rest of the surrounding intervals. A possible suggestion is that the flow direction of the water influences this, whereby the flow from T2 going to CB1 is large enough to not be affected by the opening of CB1. This would need to be cross checked with temperature studies, such as the ones by Keplikova et al. 2014, to further understand the flow directions between the fractures naturally.

Interval F1 is strange in the sense that there are 2 large fracture zone features present in the interval, yet no influences are seen hydraulically between each borehole to from either end. F1 exhibits a relatively high flow rate, which is not necessarily an indicator in the same way as transmissivity, but still hydraulic responses would have been expected here.

Fracture Feature Relation: Interval by Interval

An indepth study of Hydraulic Response rations, hydraulic data and structural data has been completed below:

Interval	Hydraulic Response Ratio	Fracture Structure Description	Fracture Structure Official Name
T5	1.3	2 Fault zones present, both in the 2 meter range. Depths 244m and 252 m. At 252 m you can see disturbance in the ATV and more black structures (indicative of a damage zone/ schist zone?) 224 m fault zone shows no ATV disturbance.	No official names
T6	2.5	1 prominent fault zone at 259 m. Strong signals in ATV, Caliper diameters and OTV.	St2_258
T7	1.3	1 prominent fault zone at 279 m. Strong signals ATV, OTV and Caliper diameters.	St2_278

T8	1.28	1 prominent fault zone at 287 m. Strong signals ATV, OTV and Caliper diameters.	St2_286

Table 1- Hydraulic and structural features based on packer intervals in ST2

These structures have been linked by R. Castilla, and it can be checked if there are any of these faults occur in CB1 or ST1 with the same hydraulic responses. The analysis from table 1 (on page 7) can be used for this with CB1, as the hydraulic intervals have been connected with the fault structures for ST2 and CB1. From the table above, the simplest correlation is that a strong response between CB1 and ST2 is that a fault zone is required.

For T5, which corresponds to the fractures in HT9 and HT8, the flow rate is 2 l/min which is not in line with the ST2 flow rates. The analysis in table 1 of the fault zone locations with respect to the fracture structures can be used in the integration of hydraulic data too.

Intervals	Hydraulic Ratio ST2	ST2 Flow Rate[1] [l/min]	CB1 Flow Rate[2] [l/min]	Electrical Conductivity Changes
T5/ HT9	1.3	0.04 (second lowest)	2.00 (third highest)	CB1: No changes ST2: No changes
T6/ HT 10	2.5	0.45 (middle)	< 0.01 (lowest)	CB1: No changes ST2: No changes
T7/ HT 11	1.3	0.21 (middle low)	0.01 (low)	Noise on both
T8/ HT 12	1.28	16.9 (highest)	9.00 (highest)	Large increases in electrical conductivity

Table 2- Comparison between Flow rates, hydraulic ratios and electrical conductivites

[1]The flow rate is the interval flow rate calculated between the packers- bucket and stopwatch
[2]The flow rate is calculated using the bucket and stopwatch method.

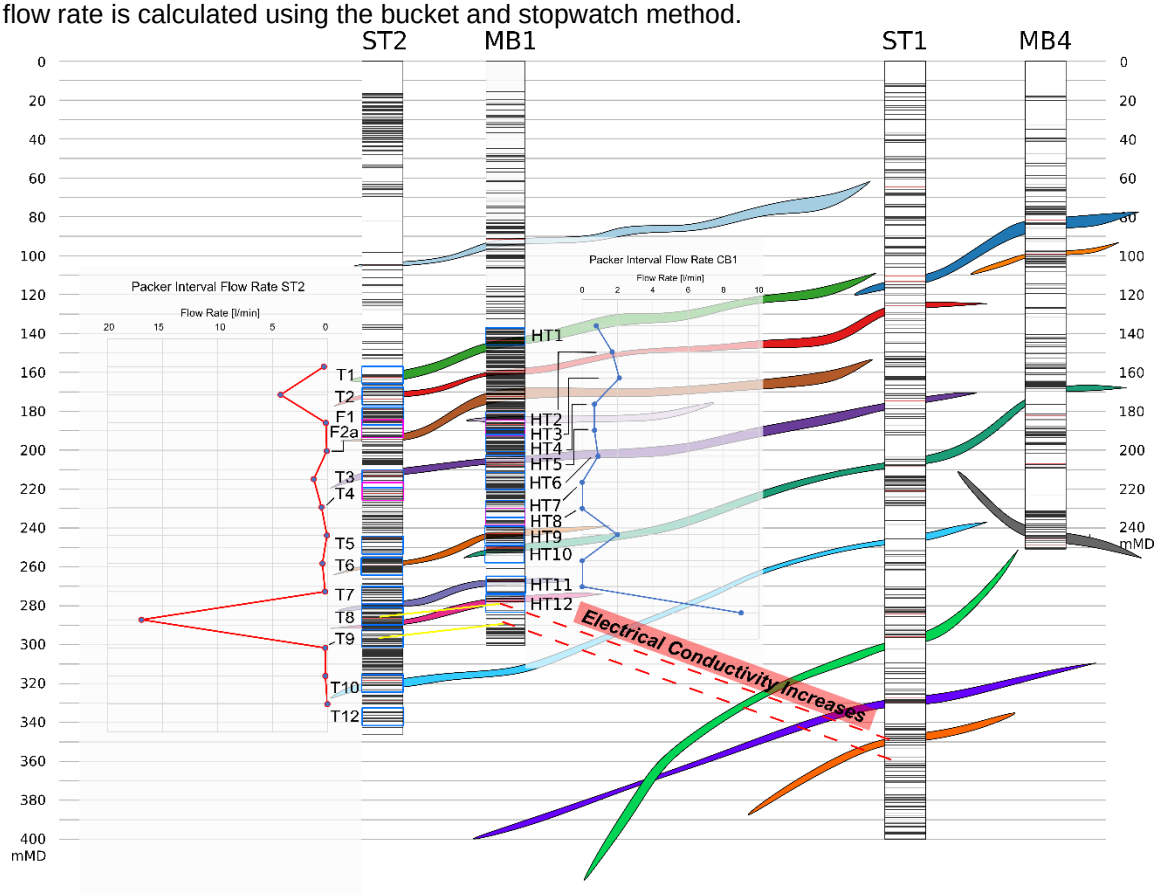

Figure 6- Interpreted fault structures (R. Castilla, 2020) with Packer interval flow rates and packer intervals labelled on ST2 and MB1. The locations of major electrical conductivity increases are also mapped on, in yellow and red dashed lines.

From the comparison of features in table 2 and table x above, T7/HT 11, T8/ HT 12 show the most similarities in the structures, flow rates and hydraulic ratios at the same time. The fracture patterns here show that there are 2 fault zones both 10 m apart in ST2 and CB1, making it fitting that the flow rates match in terms of relative positions. A more complex argument is how similar fracture structures ST2_286 and ST2_278 can have such different hydraulic flow rates but be on a similar level of hydraulic response ratios 'connectivity'. T5 shows that the hydraulic ratios do not match the flow rates to be expected; with a ratio close to 1, you would expect T5 to have a larger flow rate (see figures 5 and 6).

Looking on the flip side, **T5 and HT9** have been matched based on the relative spacing of faults on both boreholes. From OTV and ATV analysis, the fault zone in HT9 has 'less amplitude signals' shown in the ATV compared to the T5 fault zone, but this fact does not match the flow rate hypothesis, where HT9 has higher flow rates. The fault zone shared between T6 and HT10 does correspond to the orangy-brown fault plane, figure 6, and in this case T6 is the one where the ATV is more prominent and the HT10 fault almost does not show up on the ATV. This corresponds to the flow rates, **contrary** to T5 and HT9. The fact that supposed same fault zones that are relatively close together have such different flow rates is an observation.

Is there a reason why hydraulic ratios would be close to 1 but flow rates be so low? There is no direction to a rule or a model. High relative flow rates are not necessarily going to mean that a fault zone is more connected because there will be many factors involved such as permeability and porosity, for which there is no current available data.

Conclusions based of this:

- The hypothesis that flow rates will be higher for fractures/ fault zones that show defined signatures (be careful with this- a black fracture outline running the entire length through) on the ATV. Hydraulic flow rates, do not seem to be correlated with the fault extent of brokenness showed by the ATV.
- The hypothesis that flow rates will be high for ratios closer to 1, has been proved by some hydraulic intervals such as T5, to not be the case.
- Hypothesis: faults that a located closer together will share more similar hydraulic properties. This has been found not to be true on this smaller scale.

Suggestions

Collect hydraulic response testing data from tests carried out in CB1 and observed in ST2, to give a full view on the connectivity between the closely related boreholes to cross check and solidify interpretations.

There have to be more parts to the argument, possible in-depth studies of the structural and mineralogical features (microscope analysis?) of the fault zones need to be carried out in order to find a characteristic that can be used as a model.

Fracture Aperture/ Fault Thickness and Transmissivity

The calculation of the transmissivity values consequently allows the calculation of the fracture aperture, using the cubic law (Christe, Serbeto and Meier, 2020) :

$$T = \frac{\rho * g * b^3}{12 * \mu}$$

μ = water viscosity [kg/ms] ρ = density [kg/m^3] g = acceleration of gravity [m/s^2] b = fracture aperture T = transmissivity [m^2/s]

More fracture features need to be explored to suggest why the fractures in ST2 F1 containing 3 fault zones, seem to not be connected well. It is possible that the fracture aperture or fault zone thickness play a role in

this. Initial hypothesis: larger fracture zones correlate positively to larger transmissivities. The 3 fault zones range from 0.8 to 1.2, where one fault zone has almost no amplitude signal on the ATV log. Just from this example that the thickness of the fault zone does not impact the hydraulic properties significantly.

It is interesting to see whether this is followed/ there is a correlation between the fracture aperture, calculated from theory, of the damage zones, the transmissivity and the fracture aperture. This can be tested with values of fracture aperture with all the intervals. So far only interval T8 of ST2 has been tested for fracture apertures.

Therefore, a quick test on whether the Transmissivity and fault zone thickness correlate was completed, Appendix C. From this it was seen that the fault zone thicknesses between CB1 and ST2 correlated, but the transmissivities were randomly arranged. The largest transmissivities in fault zone 15 are related to a thickness that is more on the lower end of the scale. This was a very small-scale test, but it shows that the fault zone thickness and the fracture aperture may not link at all in this way too. Conclusively, fracture thickness is not something that would be related to higher hydraulic connectivity in practice.

4.2.2. Spinner Flow Meter Data Analysis

Flow through spinner logs is possible because the tunnel was drilled in the granite, this initiated the process of water drainage from the tunnel and hence large inflows of water into the tunnel. This is potentially beneficial by understanding which fractures between borehole are connected by the signals given in the spinner logs.

For ST2, the flow rate data starts at 180 m, the spinner data before this has not been transformed. The velocities up and down ST2 derived from the spinner were also calculated.

ST2:

- The background flow is around 40 m3/min.
- There are 2 noticeable large peaks in flow rate occurring at 200 m and 287 m (corresponding with interval T8) measured depths. But seems to be in the middle of a large fracture break.
- In T8, a spike of 52 m^3/min which lines up with the electrical conductivity spike and the perceived fracture associated.
- The flow is mainly considered to be going up the borehole. There are small (around 13 m^3/min) signals for downwards velocities. These mainly occur between T6 and T8.

ST1:

- The background flow is around 20 m^3/min for the spinner up flow. However, it is at -150 m^3/min for the spinner down flow. This is a significant difference.
- Wherever there are peaks in the spinner flow down, there are corresponding peaks in the spinner flow up. The only exception is between 285 m and 303 m, where a large increase in spinner down flow rate is seen and there is no signal on the spinner up log. These peaks also correspond to the fracture zones on the smaller scale.
- At 110 m there is an inflow seen from the spinner up log and the spinner down. This corresponds to the large fracture zone at 110 m observed in the OTV ad ATV (see section 4.1.1 for the naming and specific features). Likewise, peaks are encountered at 128 m, 140 m, 210 m, 220 m, 285 m.

Comparison to the Hydraulic test data

The key negatives of this comparison in ST2: hydraulic intervals will only give you flow rates through a certain interval, spinner flow rates give you the total flow rate through the borehole depending on the depth of the spinner instrument. This results on different scales of flow rates, where the spinner flow rates are much larger than the flow rates obtained from the hydraulic tests (**Appendix A**).

It is potentially useful to qualitatively check the relative flow rates down the borehole for the highest and lowest values and see if both spinner and hydraulic data show the same trends.

The hydraulic data shows a trend of the flow rates increase further down the borehole, with the exception of T2 which has a relatively high packer interval flow rate of 4.25 l/min, Appendix A. The spinner data for ST2 and ST1 shows no increase of flow rates downwards. In general, the flow rates of the spinner, high points and low points do not match very well.

Spinner Flow rates compared to the 1D Temperature logs

The main observations from ST2 and ST1 between the temperature runs and the spinner flow rates are summarized in Tables 6 and 7 respectively. Images of the logs have also been included, and the positions highlighted to show the observation depths. Figures 6 and 7 show a 1:1000 m depth scale view of these features (ST2 and ST1 respectively) identified in the WellCAD logs.

ST2				
Depth [m]	Fault Name	Hydraulic Interval	**Temperature**	**Spinner flow rate (m^3/min)**
194	**8** St2_193	F2a	Noise	Increase 40 to 48
200-204	**-**	-	Noise	Increase 40 to 60 followed by a decrease
259 (fault zone)	**11** St2_258	T6	Reduction by 0.4 °C	No signals
279 (fault zone)	**13** st2_278	T7	No Signal	Increase 40 to 45
297		T9	No Signal	Increase 40 to 52

Table 6- Observations between Temperature and spinner flow rate from ST2

ST1			
Depth [m]	Fault Name	**Temperature**	**Spinner flow rate**
110	**2** St2_162	23.5°C to 23.8°C Increase by 0.3 °C	Increase from 20 to 60 m3/min
143	**8** St2_193	Noise	Increase in up flow rate
208 - 209	**4***	Noise, series of small increases	Increase in up flow rate. But a decrease in down flow rate.
221	**11** St2_258	Increase by 0.2°C	Increase in both up, decrease in down flow rate
274		Increase by 0.2 °C	decrease in down
284*		Increase by 0.2°C	Large increase of 130 m^3/min in the spinner down (towards zero)
302* (looks like a crystalline infilled vein)		No Signal	Large decrease in 130 m^3/min in the down
330		Reduction by 0.4°C	Decrease in flow down by 20m3/min
350 (possibly linked to the fracture zone at 349)		Increase by 0.3°C	Decrease in flow down
352-354		Increase by 1°C	No signals

Table 7- Observations between Temperature and spinner flow rate ST1

*interesting intervals/ fracture zones

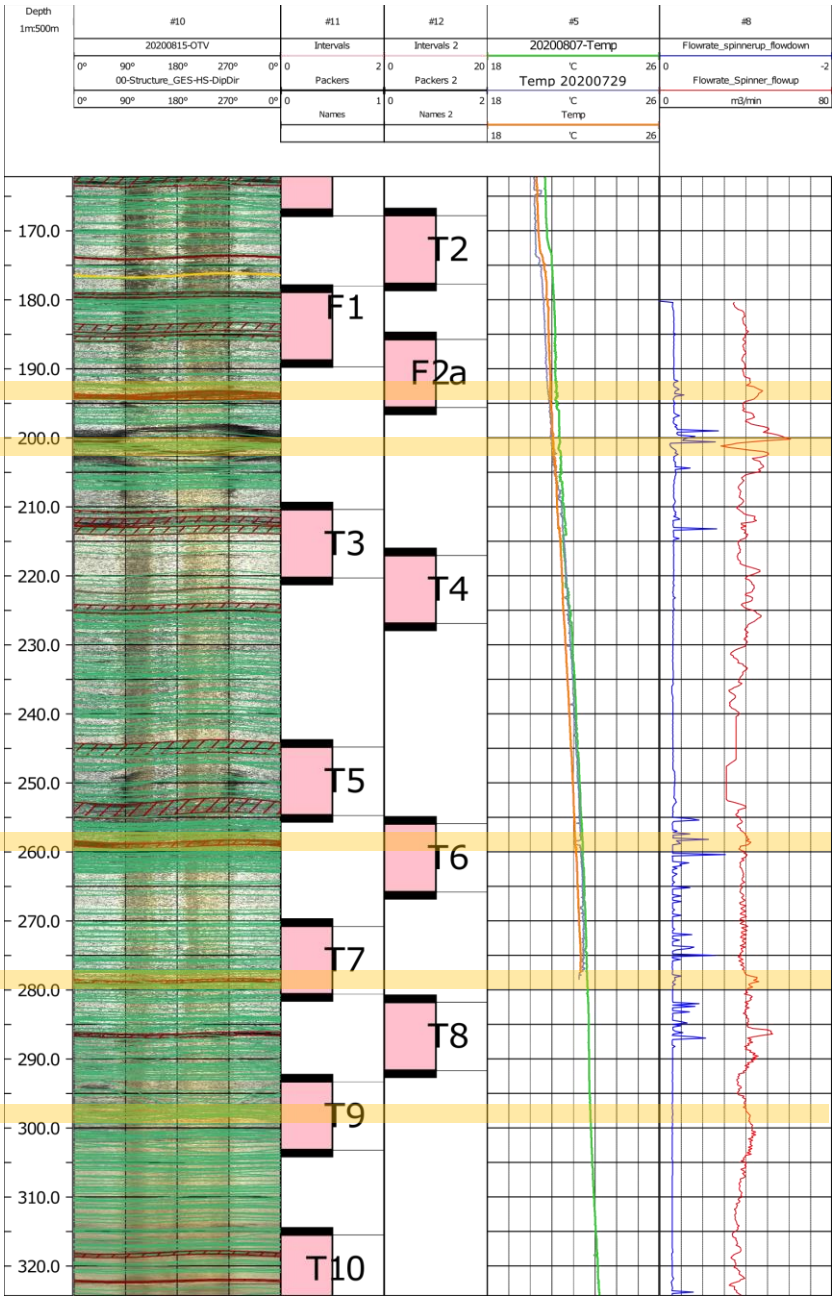

Figure 6- Composite log ST2 highlighting connections between temperature spinner and flowrate logs, for further details see Table 6.

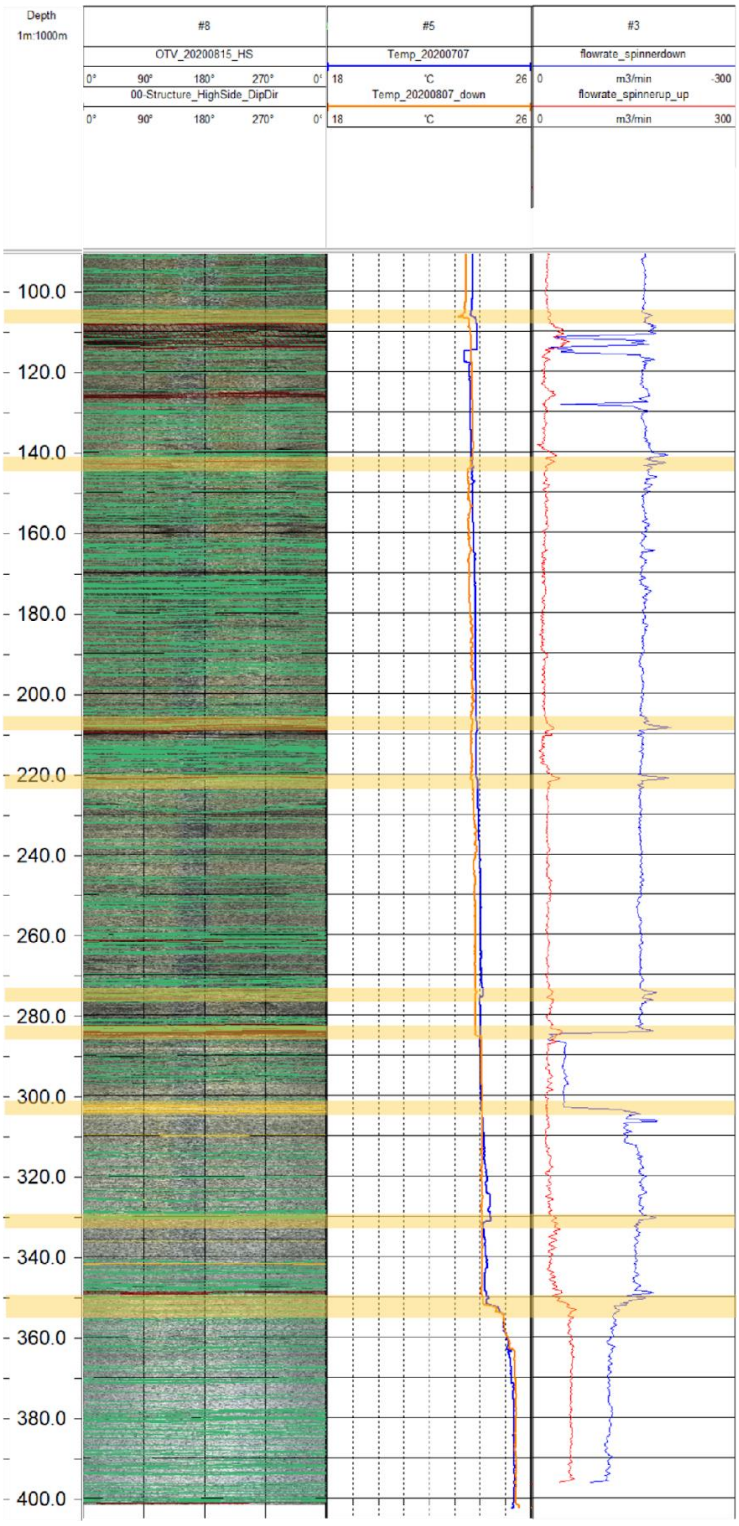

Figure 7- Composite log ST1 highlighting connections between temperature spinner and flowrate logs, for further details see Table 7.

Out of all flow rate changes, the ones at 284 and 302 m in ST1 are the largest. They relate to an outflow of water possibly related to the fault zone at 285 m and then an inflow of the same magnitude at 302 m. This is strange as the feature at 302 m is described as a mineral infilled vein which would not be expected to have water flowing through it. It is likely to be an artefact of the spinner log measurement technique for 2 reasons: the flow decreases and then increases in the same amount and the disturbance also shows up in the logging speed for which it should not if it is to do with the actual velocity of the fluid. It is likely that the spinner may

have been caught in the damaged areas of the boreholes that are due to faults, and then this would have causes a temporary drop in flow rates.

Electrical conductivity (EC) and Spinner Flow

Conductivity represents a material's ability to conduct electric current. In water, it is used as a measure of ions in solution. The SI int is Siemens per meter S/m. For deionized water at 25°C, the electrical conductivity is 0.5 µS/cm.

ST1

For ST1, there were 4 runs of electrical conductivity, and only the signatures where all 4 runs showed something are analysed in this study.

Borehole and Depth (m)	Spinner Flow (l/min)	Electrical Conductivity (µS/cm)	Structure & Orientations	Temperature
352 – 354 ST1	Increase in spinner flow down from -50 to 0. Increase in spinner flow up from -0.04 to -0.035	100- 200 increase	No Fault zone association, but there is a fault zone at 349 m (ST1_349). The orientations in this unit are 2 main ones: one striking NW-SE, and another NE-SW. Dip angle is around 70°	1°C increase
359 – 363 ST1	Spinner flow down stays at around 10 l/min. Spinner flow up stays at -0.04 l/min.	80 – 180 increase	The structures are mainly individual fractures. The orientations in this unit are 2 main ones: one striking NW-SE, and another NE-SW. Dip angle is around 70°	No Changes
286 -287 (T8) ST2	Signal, big increase that runs the span of the fault zone- increase up to 350 l/min (flow down unrealistic)	50 increase	Fault zone ST2_286 is associated with this change.	No changes.
300 – 303 (T9) ST2	No change in flow up or down. (flow down stays at 190)	80 increase	Many individual fractures that are density packed together. From 300 -302 thee is as what looks like darker mica bands? Indicating shear zones?	No changes.
173 – 174 ST2 (T2)	No data	75 increase	There is a fault zone directly associated ST2_174. Orientation: (NE-SW) 333/76°	0.2°C increase
277 – 278 CB1 (HT 12)	-	100 increase	Directly associated with a fault zone CB1_278 345/72°	No changes
290 CB1	-	80 increase	No fault zones, just small individual fractures. (Need to recheck the structural orientation)	No changes

Table 3- This data can be viewed side by side in the composite logs. Red = upper EC changes, Blue = lower EC changes wrt boreholes.

In most cases a change in electrical conductivity is not associated with a change in temperature. When it comes to spinner flow shows that the ST1 data shows that there are increases in flow where changes of Electrical conductivity occur. This provides evidence that flow into the borehole is the source of the change in

ionic content and that there are different types of water flowing through the 300 – 400 m section of Rotondo granite.

Is electrical conductivity associated with a change in structural orientation? Is there a structural feature that can relate all of the electrical conductivity increases?

In most cases a change in the Electrical conductivity of a borehole is not always associated with fault zones. However, the intervals HT-12 and T8, show that electrical conductivity increases of 50 – 100 µS/cm are occurring along the same fault structure. (More links are shown in Table 1). The structures orientations can be factored in as well, most changes occur with the structures that have a NE-SW orientation (the general orientation in all boreholes). In the case of T9, there is no fault zone however there are densely packed fractures some of which correspond to the NW-SE orientations, and it is possible that the increased electrical conductivity is related to these structures. On the flip side in HT-12, which is spatially close to interval T9, there are very few individual fractures and a fault zone that is orientated NE-SW. There are structures that dip SE instead of NW, figure X, but the depth of the electrical conductivity increase is located exactly at the depth of the fault zone. So, there is evidence that electrical conductivity changes at fault zone structures, but the effect of smaller structures also contributes.

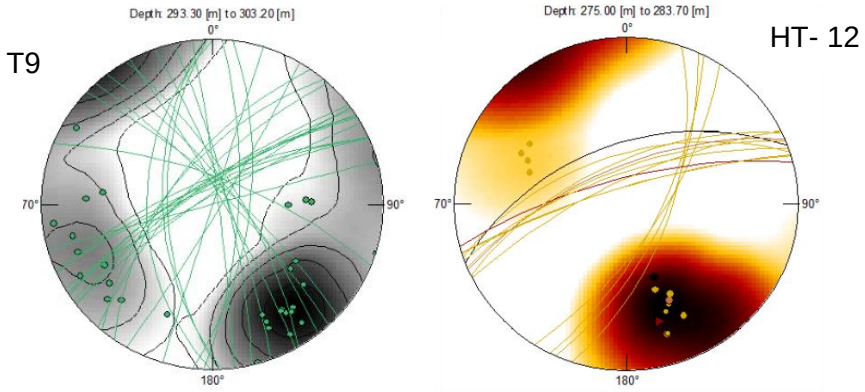

Figure 1- (left) Stereonet of structures in T9. (right) Stereonet of structures in HT-12

From the depths, it appears that for CB1 and ST2 the EC change occurs at depths of around 280 m, for ST1 this occurs at the depths around 350 m. This could represent a change in water compositions thus relate to a structure. In each borehole at around these depths are 2 consecutive electrical conductivity increases, but not all of them are associated with fracture structures. There is a trend however, in ST2 and CB1, the **upper EC change occurs with a fault structure (T8 – HT-12)** and the lower change occurs in individual fault structures. For ST1 it is possible for the upper EC change to be related to a fault structure, but this is not linked by R. Castilla, 2020 in figure 4 (pink fault) as the same structure in ST2 and CB1- it is the lowest orange structure instead (figure 4). The lower EC changes all occur in individual fractures or clusters of individual fractures, as seen on the figure below.

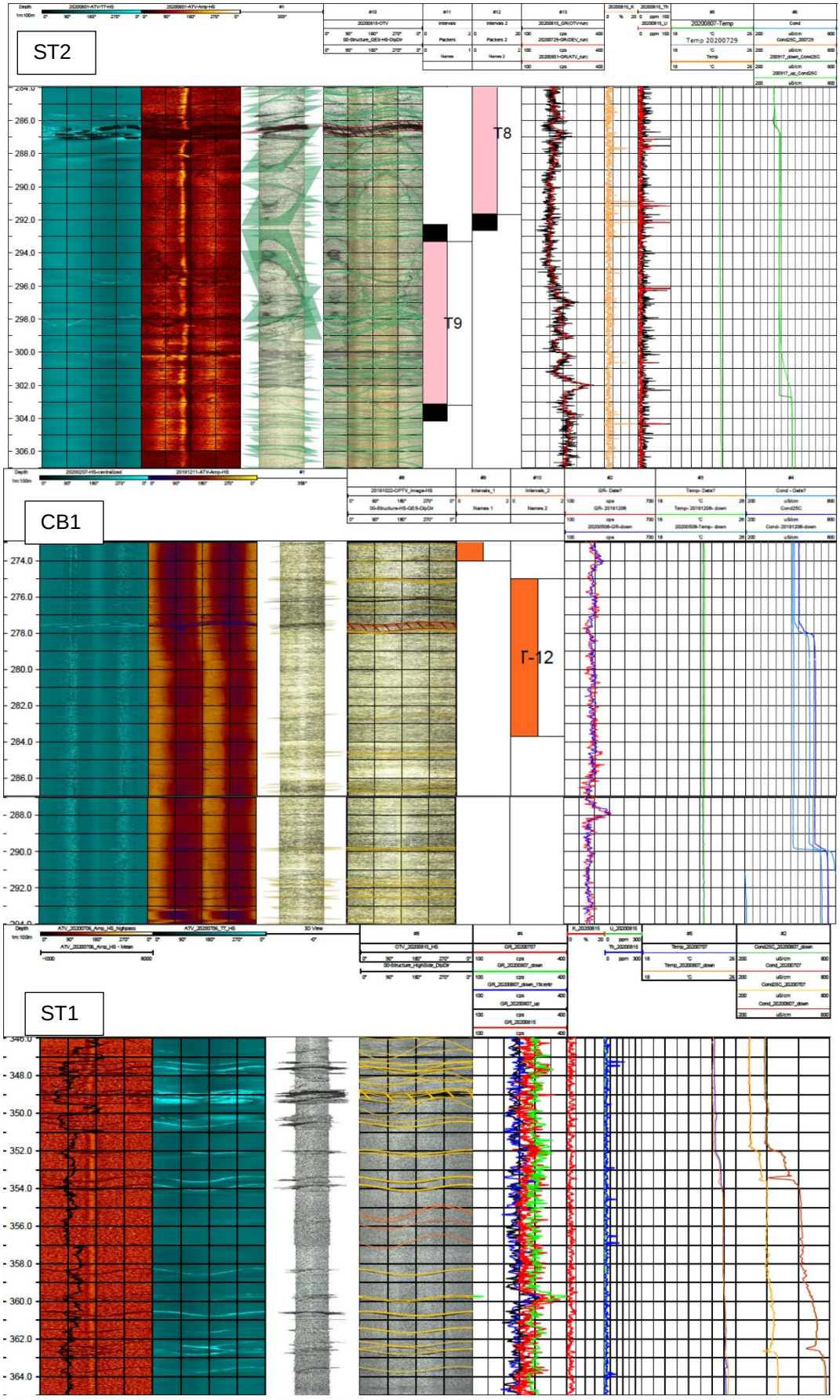

Figure 2- Sections of log from ST2, CB1 and ST1 showcasing the 2 major electrical conductivity jumps in each borehole, with respective depths and temperature changes.

Is EC linked to the different orientated structures seen in ST2 T8 which leads to higher flow rates?

None of the electrical conductivity increases properly match the paired hydraulic packer intervals. This potentially says that the transmissivity or the flow rate of a structure does not correspond to more concentrated ions flowing into the borehole. If T2 is considered, as the electrical conductivity spikes here too (table 3), flow rates are also high from the associated fracture zone. So, interval flow rates are higher in the fault zones that experience EC changes.

Does the spinner in ST1 show greater flow rates for the structures at 330 md? At 350 the flow rates increase from the flow up results. At 350m the flow rates increase from the flow down results as well.

Conclusions:

- From the evidence in CB1, ST2 and ST1 it can be said that a change in temperature does not affect the electrical conductivity in the boreholes.
- It is likely that a change in EC conditions reflect a type of 'boundary' at the lower levels of all 3 studied boreholes, shown by the integrated figure X (1 is the wrong no.)
- There is enough evidence to say that for most structures in all 3 boreholes, an EC increase relates to a fault zone will have higher flow rates, shown by hydraulic interval flow rates and spinner flow rates.

Proposed model- is there a different type of water circulating at the bottom? Is it possible to relate some of the changes to the hydraulic data? Or is it more likely to fit gamma ray data?

The spinner flow rates and the temperature (20% for ST2 and 60% for ST1 of the time ~rough estimates) have some sort of correspondence. The spinner data from ST2 fluctuated more than in ST1 and was harder to read than the ST1 spinner data, hence less connections between the temperature logs were distinguished. Overall, the data in tables 6 and 7 above that can be related spatially using the methods adopted by Klepikova et al. 2014, illustrated in Figure 9. A 2D model using Leapfrog or Hydrotherm software is possible to create a model of temperature and water flow from the fractures.

Suggestions

Another Spinner test in ST2 should be run to obtain better quality data to interpret.

2D Temperature Logs

By utilizing temperature tomography logs it is possible to view in detail temperature between the boreholes that can give more information into how the fractures connect and possibly the type of fracture node connections if they exist.

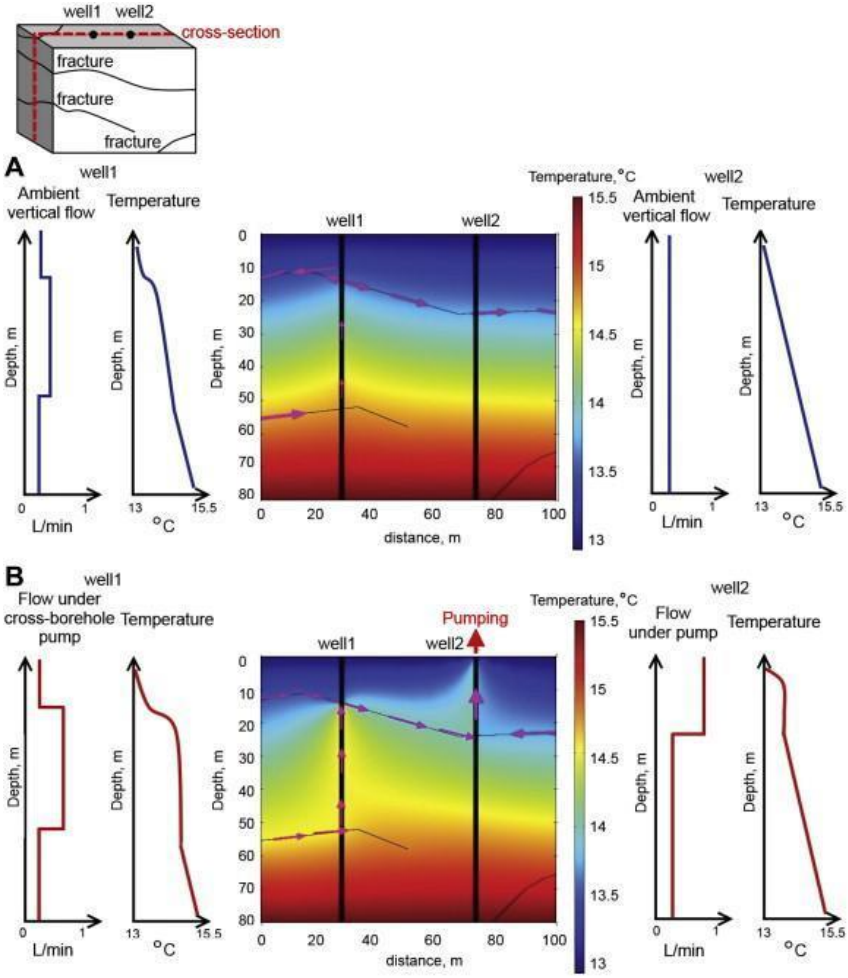

Figure 9- Passive Temperature tomography between 2 boreholes where the corresponding temperature and flow logs are displayed by Klepikova et al 2014.

There are a few possible methods to explore this observation/hypothesis further:

- 3D structural analysis to see if the 2 ‘fault zones’ are on course to collide or run parallel.
- Investigating in terms of fracture networks this could be described as a Y- node, Figure 8 but further specific research would be required. However, these signals were picked up by the spinner down and not by the spinner up run, which poses the question if this is a true observation or a fault of the apparatus.

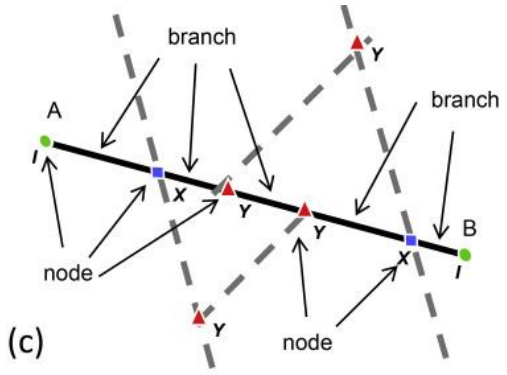

Figure 8- Node Branch 3D models where the fracture tips (green circles), abutting fractures (red triangles) and cross cutting intersections (blue squares). (Sanderson, 2019)

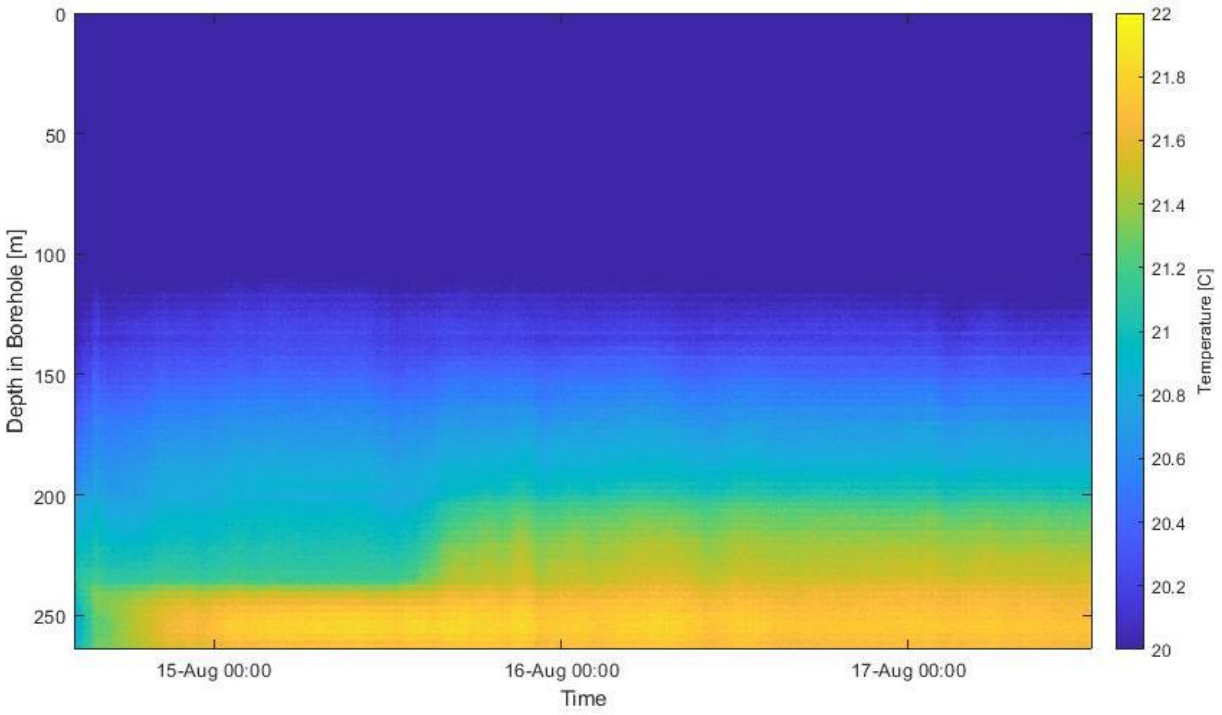

Figure 3- Ambient Temperature Tomography of CB1, during closure of all surrounding boreholes

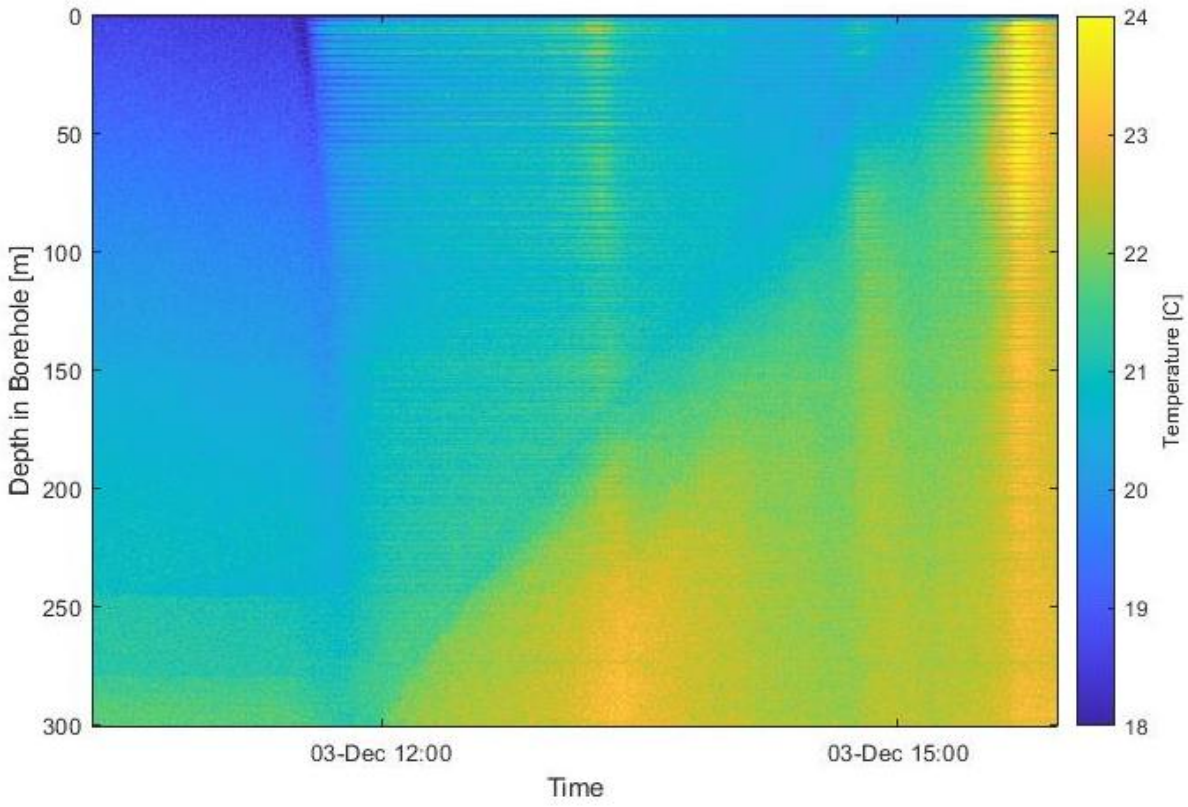

Figure 4- Temperature tomography of CB1 during the cementation process.

4.3- Geophysical Data Analysis

4.3.1. Gamma Ray Data

There were not many literature sources to review the analysis of gamma ray logs in igneous environments.

- In the Grimsel Lab, GR runs as well as Spectral Gamma rays were taken, however the data has not been discussed in found published papers. (Source: https://doi.org/10.3929/ethz-b-000243199)
- The SKB (Swedish Nuclear Fuel and Waste Management Company) completed Geophysical borehole logging within its boreholes, but despite having GR data, it was not analysed for specific features. (Source: https://www.skb.com/publication/1984243)

(Average in other granites is around 180-220 API units (American petroleum institute))

ST2:

1. Peaks, when present are broad, the background is at 200 cps. The largest peak is seen in T2 and T9.
2. The places where fractures present to intersect GR spikes can be due to fracture infilling material. T9 appears to have some fractures that are closed and possibly infilled from the ATV analysis.
3. Between the intervals T6 and T8, the GR cps reduced to 250 cps and there is less fluctuation in the cps.
4. T9 – T12 has gamma ray data constant at 250 cps, again with less fluctuation in cps.
5. The zone between F1 and T3 has large outbreaks seen in both the OTV and ATV viewers. This seems to cause great variations in the gamma ray data.

CB1:

1. The background radiation is around 300 cps.
2. There are zones of increase at measured depths: 100 m, 138 – 142 m, 170 – 180m related to a fracture zone, 210 – 217m and 227m.

ST1:

1. The background radiation is 250 cps.
2. Each run is quite random, noisy, and large increases in cps cannot be directly linked to anything on the OTV and ATV.
3. At 303 m, there is a visible change in colour of the rock from the OTV which results in large increases in excess of 400 cps. The P-wave significance is discussed in **section 4.3.2.**

Interpretations

The reduction between T6 and T8: There are fractures oriented NW-SE which brings the likelihood of different water sources, with different concentrations of radioactive particles. So, it is a possibility that the water from here contains less radioactive particles. This also fits with the electrical conductivity conclusions stated in section 4.2.2. There is the potential for more in-depth analysis, using mineralogical studies of Rotondo Granite samples.

A final note is that it is not possible to attribute peaks in GR or spectral gamma to individual fracture zones, like it is with P-wave data. Even though CB1 and ST2 are close together, the gamma ray logs do not correlate well. It is possible that the peak at 160-170 m in CB1 relates to the peak in T2, but there is little ground in this, as the scales are different.

There is little value in using gamma ray to compare logs from different boreholes, because only to radioactivity from the surface of the boreholes will be picked up. In addition, there would be a lot of variation laterally across from borehole to borehole.

Suggestions

By measuring a 300 m interval of granite rock, it seems unlikely that granitic 'lithological' changes will be seen. A bigger understand of the larger scale geology of the Rotondo granite needs to be seen to know if there is as much homogeneity as expected. It is more likely that greater changes will be seen over the kilometer scale.

Usually, it can be expected that thorium peaks are seen in the fracture intervals where water would be running, but in the cases of ST1 and ST2 and CB1 these were not seen at all. Better data needs to be collected in order to distinguish something useful from it.

It is possible that GR logs can be used in scenarios of actual hot rock where the granitic lithology contributes to generation of radioactive heat, such as the situation in the Cornubian batholith.

Alternative Methodologies

Since it was very hard to correlate gamma ray logs, with respect to depth, with single fracture structures. It may be possible to correlate the more general fracture densities, or groups of fractures to an increase in gamma ray transmission. Particularly with Uranium emissions, the fractures/ fault zones with higher permeabilities can be detected. This is because most uranium compounds are soluble in water, therefore are more likely to be present and precipitate in these more permeable zones with higher water flow.

1. Every few meters take the mean value of fractures/ fault zones in the interval and take the mean gamma ray values of the interval.
2. Do this for all the boreholes and then see if there are any correlations in this way.
3. On WellCAD is it possible to do heat maps?

4.3.2. P-Wave Analysis

P wave signal analysis

The P-wave RX filtered stackings have been used to cross check the locations and the size of a fault zone/ fractures in ST1 and ST2. Most disturbances where the stacking becomes 'white' is when the waves intersect a fracture/fault zone. The extent of the disturbance has been correlated to the depth/ size of the fracture zone; larger ones have stronger signals.

An interesting observation was that for ST1 at 304 m measured depth, figure 10, where there was a visible semblance disturbance that was about the same thickness of the aplite dyke. It is possible that the P-wave velocity through granite and through aplite dykes are large enough to be seen in the logs. There is a distinct gamma ray peak too which re-enforces that at least the mineralogy of this labelled fault zone is different. The P-wave semblance stacking occurs at a depth 3 m below the depth of the aplite dyke feature.

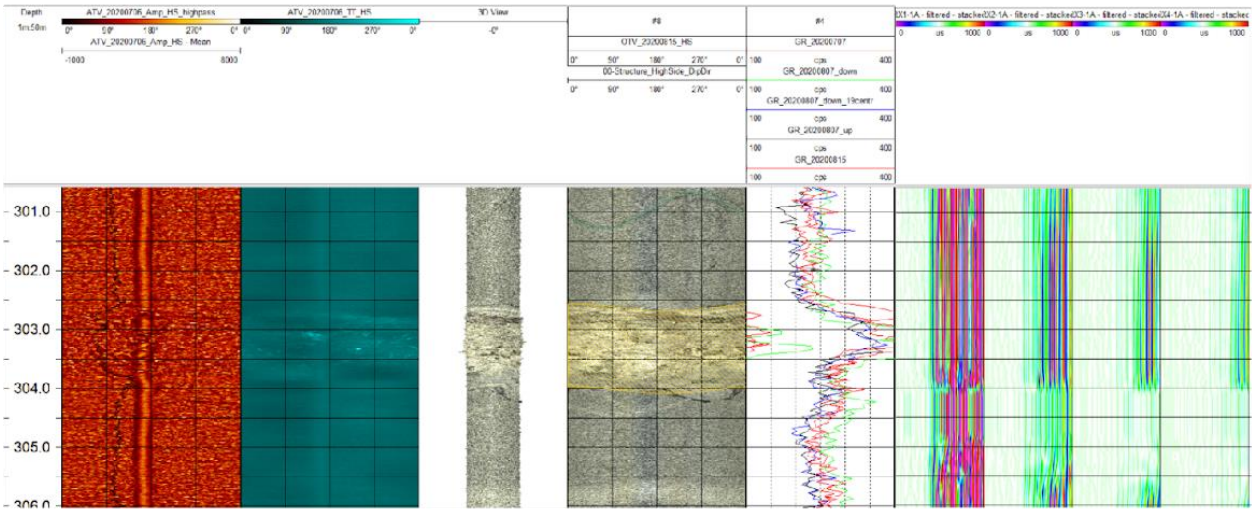

Figure 10- Borehole logging view of infilled vein feature at 302.5 to 304 m depth in ST1.

P wave velocity analysis

The detailed picks of the P- wave arrivals can be correlated to the cumulative fracture frequency. Where there are increase in fracture density (large gradient increases), P-wave velocity changes (reductions) are seen, Figure 15.

The P-wave velocity graphs with the initial P-wave peaks are shown for ST1 and ST2 in Figures 11 and 12, along with the fault names and fracture density stick diagrams that correspond to the fault zones and the perceived P-wave velocity reductions.

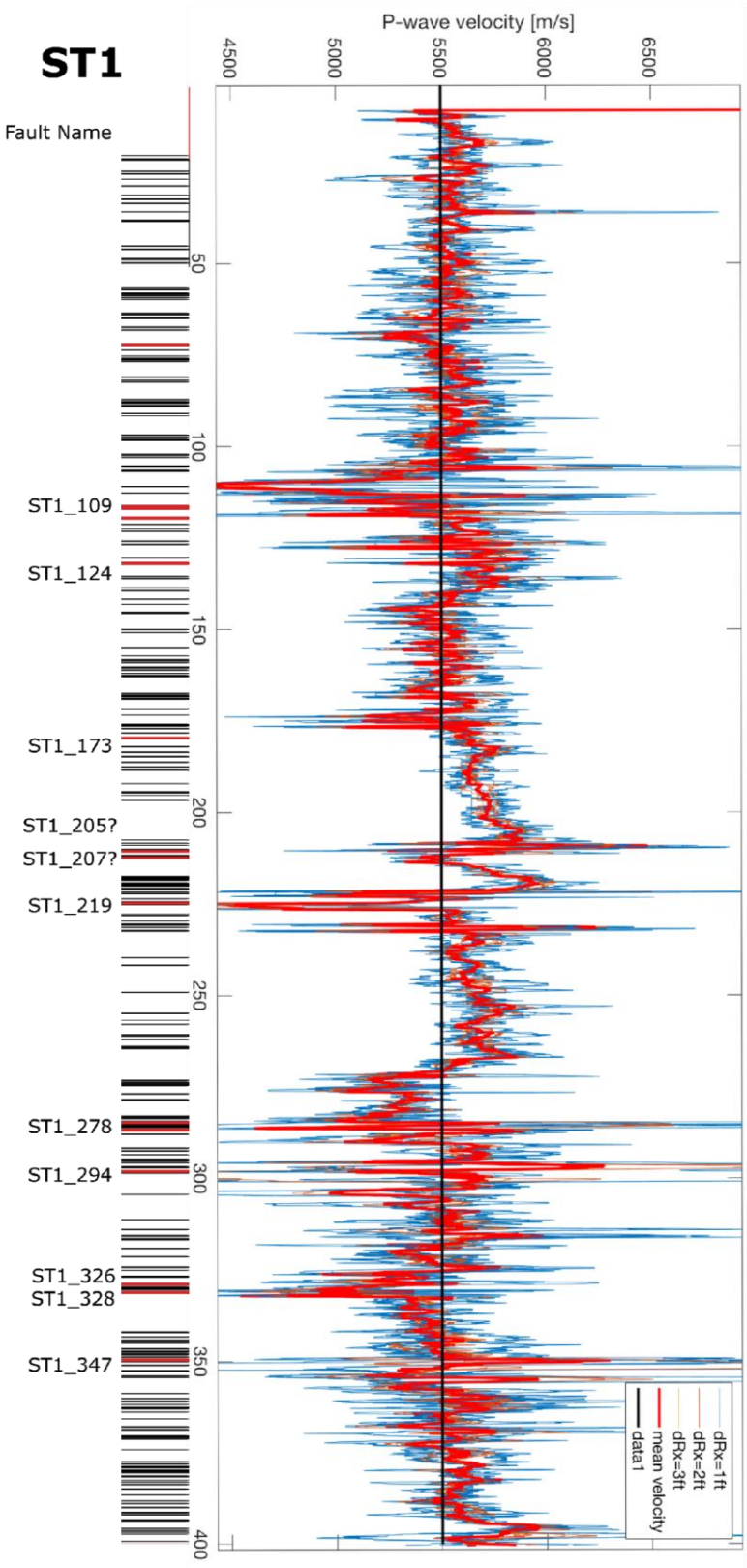

Figure 11- P- wave velocity graph for ST1 with connected fractures added on, indicated by the numbers. Stick diagram with fault zones indicated in red, taken from R. Castilla, 2020

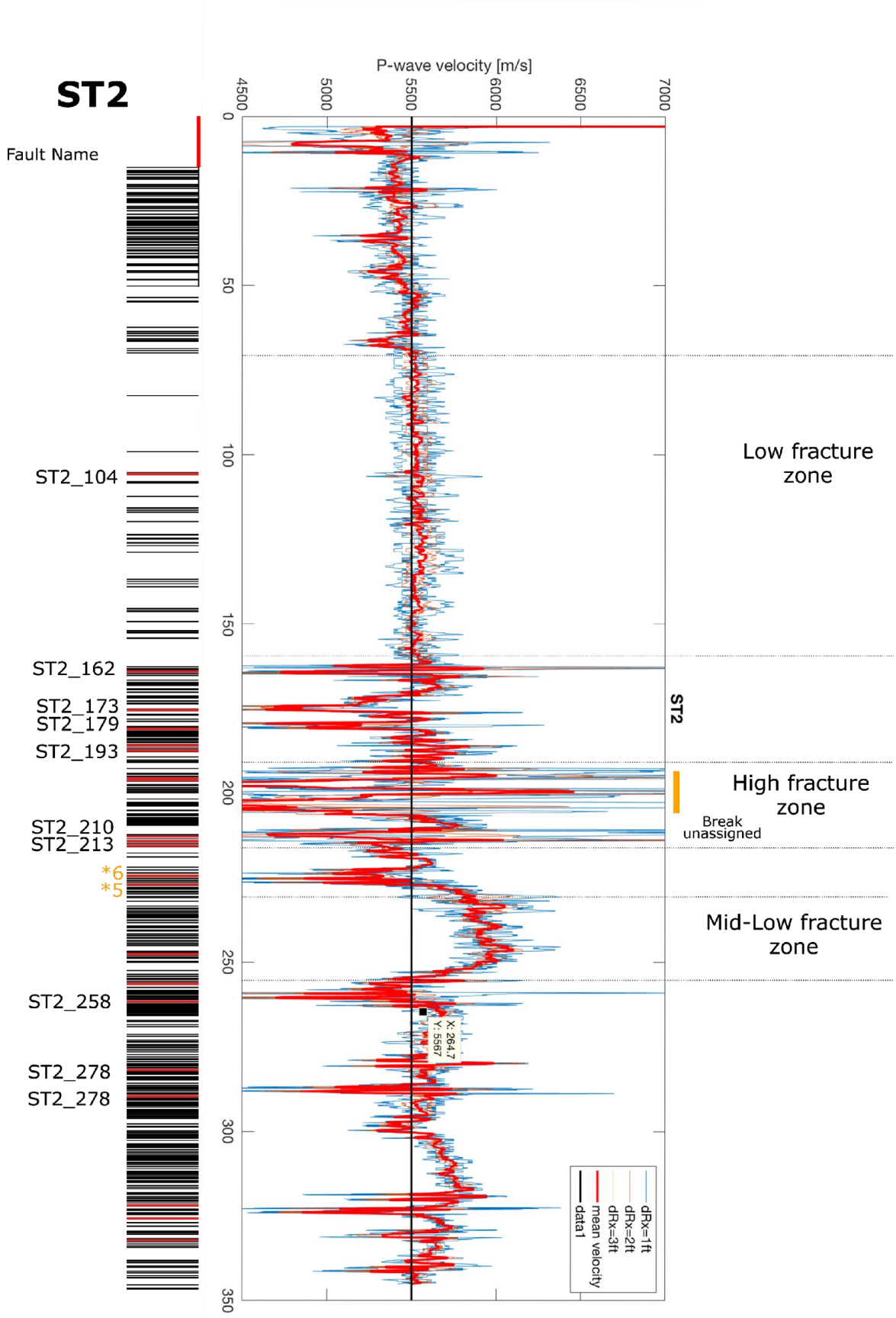

Figure 12- P-wave velocity graph for ST2 with connected fractures added on, indicated by the numbers. Stick diagram with fault zones indicated in red, taken from R. Castilla, 2020

ST2		ST1	
Fault Zone	Mean P-wave Velocity [m/s]	Fault Zone	Mean P-wave velocity value
ST2_104	5500	ST1_109	4400
ST2_162	4750	ST1_124	5650
ST2_173	4700	ST1_173	5150
ST2_179	4700	ST1_205	5700
ST2_193	5500	ST1_207	5800
ST2_210	5500	ST1_219	5950
ST2_213	4750	ST1_278	5250
ST2_258	5500	ST1_294	5600
ST2_278	4800	ST1_326	5700
		ST1_328	5200
		ST1_347	5450

Table 8- Mean P- wave velocities for each labelled fault zone in Figures 11 and 12. Values labelled in red indicate P-wave velocities above 5250 m/s

Interpretation

The P-wave data indicates that down the borehole, there are structures that are filled with voids that can be interpreted as fractures. It can be seen that the P-wave velocity data from ST1 is significantly noisier than from ST2, which is reflected in fact that it was harder to clearly identify fault structures than in ST2. In fact, without the structural data from the stick diagrams, significantly less fault features would be distinguishable. If the implementation of P-wave velocity data in boreholes yields noisy data, the opportunity for good interpretation is reduced to a level which would not give any detailed knowledge of the overall borehole structure.

There is a valid case when it comes to misidentifying fracture features with infilled fracture features that are also present across a borehole. In ST1, the Aplite dyke appeared to have large enough P-wave velocity differences to be picked up like a void filled structure in the log. Therefore, P-wave data needs to be used in relation to other data sources to give reliable data of fracture structures in a borehole. This is discussed in section 5.

Threshold attempts for the P-wave velocity reduction to result in a fault zone have been made from analysis of figures 11 and 12. The Mean P-wave velocity was noted for each labelled fault zone, and the results shown in Table 8. The mean velocity was used instead of the dRx = 1ft, 2ft, and 3ft values, as it incorporates this data with less noise. The ones labelled in red show values that were above the overall mean, and thus did not show velocity reductions. From these values, a threshold of 5250 m/s can be initially proposed for a fault zone to be present.

Issues with the analysis: the P wave semblance analysis shows that all the signals slightly offset from the fracture features (not just the aplite dyke mentioned before), and from comparison in WellCAD, the same goes for P-wave velocity. This is a problem as seen in Figures 11 and 12, the velocities values vary greatly over short distances.

Suggestions

Studies where the aplite dykes and quartz veins have been mapped on stick diagrams down the borehole can be cross checked to see if these areas also exhibit increased P wave velocity to any extent.

5. Combining P-wave, Drilling Data and Fracture Density

Figure 15 shows the relationship P wave velocity, drilling progress and cumulative frequency. When high density zones of fractures are encountered (gradients are increasing), the P-wave velocities reflect this with reductions in velocity. In ST2 this can be seen most prominently at depths 161 m, 180 m, 204 m, 224 m, 260 m. The zones where the connections are more apparent have been highlighted in yellow on figure 15.

This relationship can be also viewed by creating cross plots and looking for a linear trend to see the extent that the data is consistent. Figure 13 shows a cross plot for ST2 where there is a trend whereas the p wave velocity reduces, the drilling progress increases, shown by linear fitting equation. Figure 14 shows the cross plot for ST1, which is noticeably nosier than ST2. This was expected as can be seen in figure 11, where the P-wave data for ST1 is also noisy and where fracture connections were harder to identify. For both boreholes a negative linear correlation is seen.

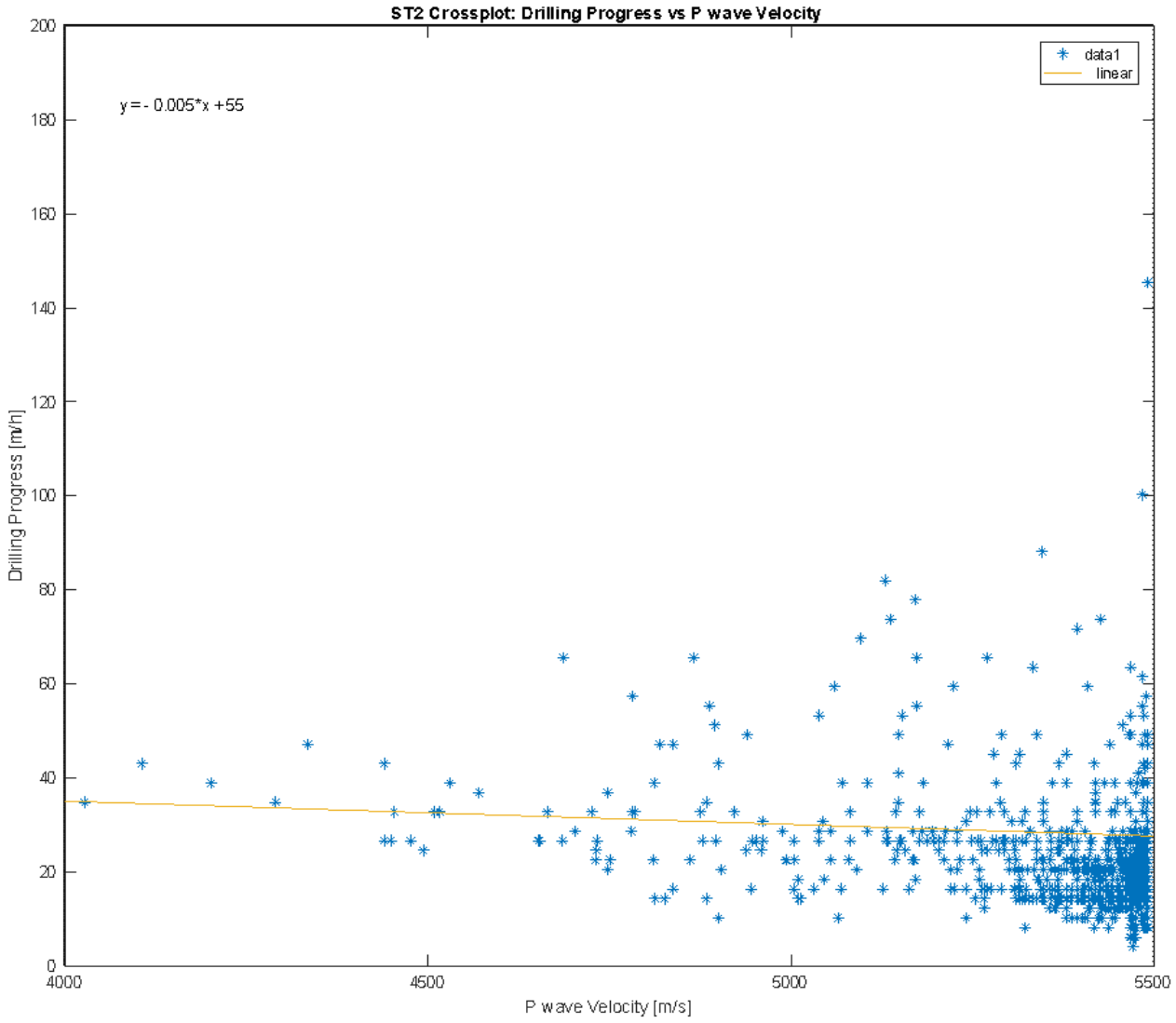

Figure 13- Cross Plot showing the Drilling Progress against P wave velocity for ST2

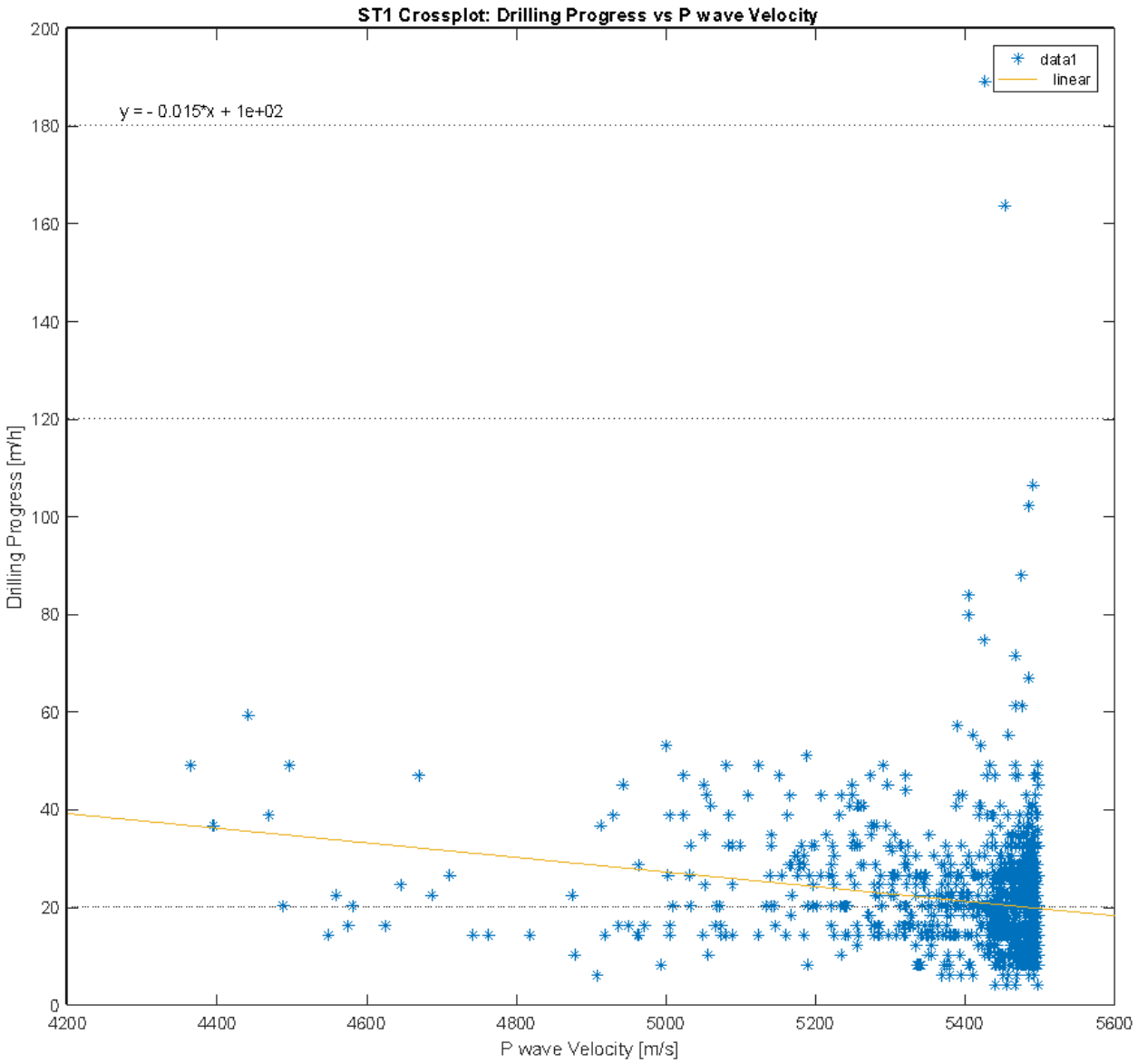

Figure 14- Cross Plot showing the Drilling Progress against P wave velocity for ST1

Interpretation

The Drilling Progress peaks clearly match the OTV images especially when viewed at a high resolution, **Appendix D**. Analysis of the P-wave, drilling and fracture density data shows that there are links and similar trends in noise that can be attributed to fracture connections. In both the drilling data and the P-wave data, the same peaks could be identified that corresponded to fractures, table 1. To some extent, the fracture zones were seen more easily in the drilling data, whereas not as many connections could be distinguished in the P-wave P-velocity graphs and semblance stacking. The P-wave stacked and filtered semblance data shows the vertical extent of the fracture zone outbreaks better than the drilling data, as it is possible to see the interference in the stacks more clearly. It is possible that drilling data can be used along with OPTV/ATV geological interpretations to get very similar results to using P-wave data Electrical conductivity and temperature runs in addition. The P-wave data (semblance and velocity) alone cannot be used to determine fracture zones, as it was seen that there are other features such as aplite dykes picked up in the logs which could lead to misinterpretations more easily than with the Drilling Progress.

From figure 15, the correlated areas were highlighted in yellow. Most times it is clear to see the drop in P-wave velocity and spikes in Drilling Progress, however in high fracture density areas it is more useful to look at higher

resolution WellCAD logs to see the peaks/spikes, for example from 275 to 300 m in ST1 and 150 to 200 m in ST2.

Overall, it was observed that the correlation between the Drilling data and P-wave data by knowing Structural connections between ST1 and ST2 prior (Figure 2), matched in Table 1 around 90% of the time, where sometimes there would not be a Drilling spike in one borehole, but a P-wave signal would be present, as in the fault zones: ST2_210, 11* and 6*.

6. Conclusions

This report shows that through integration of all the data sets many different types of correlations between the boreholes ST1, ST2 and CB1 can be identified and there are a range of methods available in order to do this. The integration was done between parts of data that could be contrasted and compared realistically, such as comparing temperature and spinner flow logs together, the same goes for fracture density, P-wave data and Drilling data. Then to attempt to integrate the full data sets, the results of the initial data combinations were compared together.

What was seen is that even though many pieces of data fit together in borehole, e.g. electrical conductivity, temperature, gamma and fracture, the same fits were not seen in the same supposed fracture in another borehole. This was for some time problematic to interpret as one would expect similar electrical conductivity jumps in the same fracture, especially within closely drilled boreholes; ST2 and CB1. Therefore, individual data sets, e.g. electrical conductivity or temperature logs alone were not enough to identify fracture trends/ characteristics between boreholes and further approaches needed to be taken. In this study the strongest evidence for integration of data between borehole fractures came from following methods:

Combination of Drilling Data and P-wave data

The main question with the use of data from ST1 and ST2 was: is it possible to use the Drilling data to estimate the locations of fracture/ fault zones? The findings showed that it is possible to use the Drilling data to estimate locations of fractures to the meter to decimetre scale. These often occurred as sharp spikes and were relatively consistent to use on their own matching to structures in 70 – 80% of cases. When considering the analysis of the Drilling data with the P wave data with prior knowledge of the connecting fracture zones in table 1, the matching percentage was higher at 90%. It was decided that the OTV and Drilling progress alone would be enough to identify fault zones, where the P-wave data did not add so much more information, apart from a possible indication of the scale of the fracture zone. However, when one has access to OTV logs, identifying fracture thickness from this is more effective.

Hydraulic Response Ratios and Structural Orientation and Flow Rates

From the ST2 and CB1 hydraulic test reports by F. Christe, F. Serbeto and P. Meier, it was concluded that the fractures connect hydraulically especially in the zones T5 to T8 where wellhead flow rates and transmissivities are higher. This is in accordance with what would be expected as higher transmissivities meaning that more water will flow through these fractures with time. The ratio calculations of the responses from the Pressure-Time graphs support this conclusion. From the ratio data, in ST2 it appears that the connectivity increases with depth with CB1 exerting more hydraulic influence from T5 to T8, seen in Figure 4.

The fact that there is a vertical fault zone present in T8 (Figure 3B), which was the interval with the highest packer interval flow and transmissivity suggests that vertical pathways may be the favorable for water to flow through the most. However, this was also found to be in a region with a change in structural orientation from NE/SW strike to NW/SE. This can therefore be investigated further with 3D analysis and in detail hydraulic testing to see if this fracture zone is the cause of such large flow rates or not.

The hydraulic intervals were matched and the fault zones were analysed spatially and with respect to ATV, hydraulic ratios. It was concluded that the hypothesis that flow rates will be high for ratios closer to 1, is not the case as seen from T5 – flow rates were not high here, and also T2 where flow rates were high but no hydraulic response was measured. Another hypothesis was that the faults that were located closer together would show similar hydraulic properties, if the faults were similar in the OTV and ATV and were matched to faults in other boreholes. This was the case for some faults such as the ones shared between T7/HT 11 and T8/HT12, but not all of them. The reason why it does not work for all based on this borehole data is yet to be explored further.

Combination of Temperature and Spinner Flow Data

It was found that temperature runs can be useful in comprehending the inflows and outflows across the multiple boreholes, coupled with flow data that was calculated from spinner runs. From the spinner data, a beginning for fracture inflows and outflows between fractures were made, such as in ST1 between 284 m and 302 m.

The spinner flow rates and the temperature have some correspondence (20% for ST2 and 60% for ST1 of the time ~rough estimates), but this was seen to be heavily influenced by the quality of the runs.

Therefore, the methods require accurate and good experiments to be run. But for further analysis, the construction of 2D temperature tomographs would be necessary in visualizing the data to achieve fracture connections.

Further combinations with Electrical Conductivity and structural orientations

Attempts were made to incorporate hydraulic ratio, flow rate, spinner data, structural orientations and electrical conductivity together, partially shown by figure 6. It was found that electrical conductivity and temperature do not have strong correlations between them in the boreholes. All 3 boreholes had distinct electrical conductivity changes at lower depths in the boreholes, (280 – 350 m in each borehole, figure 3) which is plotted on figure 6 as a zone. This change does not reflect the NE- SW orientation of the major faults as seen on figure 6, but works in another way- possibly the smaller structures in ST2 could also be involved. This would result in a EC 'boundary' indicating different flow paths for water to be present. It can also be concluded that EC changes are likely to be accompanied by a flow rate change, as this was seen in the packer and spinner flow rates. Another observation made with the Gamma Ray data was that there is an overall reduction in gamma ray from T6 to T8, which could work in support of this. More analysis on the gamma ray data with the relevant calibrations are thus needed.

Making a model

From this analysis, the reservoir can be characterized as having the majority of hydraulically connected faults located deeper (~300 m depths) in the boreholes, where flow rates are highest which also corresponds to largest electrical conductivity increases. This hints that a different 'water types' flows through there either connected to the main fault structures or the flow in the NW-SE orientated structures.

7. Evaluation

On reflection the integration of the Fault Zone structures with Drilling Data and P-wave analysis, table 1, was ambitious. The method was not effective in reinforcing the fracture connections from structural analysis for a few reasons:

4. The Drilling Progress spikes relate to an area where drilling occurred at a greater rate; it was hypothesised that this occurred due to fracture zones. The magnitude of the spikes have not been found to relate to the size/ thickness of the fracture zone. Therefore, it was only the presence of an increase in drilling progress that could be noted, which inferred a fault/fracture zone. This is not of much use as the structural analysis had already established that there was a fault zone present in that location.
5. The strength of the P wave semblance stacks, match between the boreholes for a small extent, but due to the size of the sample, this does not give any meaningful correlations. It is still only a hypothesis that needs to be statistically analysed.

Tasks Remaining:

The temperature tomography potential

Exploring the Gamma ray with calibration

Exploring the P – wave data with Gamma ray

8. References

Sanderson, D. J., Peacock, D. C., Nixon, C. W., & Rotevatn, A. (2019). Graph theory and the analysis of fracture networks. *Journal of Structural Geology*, *125*, 155-165.

Klepikova, M. V., Le Borgne, T., Bour, O., Gallagher, K., Hochreutener, R., & Lavenant, N. (2014). Passive temperature tomography experiments to characterize transmissivity and connectivity of preferential flow paths in fractured media. *Journal of Hydrology*, *512*, 549-562.

GES Internal Reports:

Christe, F., Serbeto, F., Meier, P. Evaluation of hydraulic tests in borehole ST2 and Hydrotest tables. Report date: 30.09.2020. Internal Report.

Serbeto, F. and Meier, P. Evaluation of hydraulic tests in borehole CB1. Report date: 18.12.2019. Internal Report.

Raymi Castilla Figures: GPR fault zone structures, Figure of all structures and fault connections across boreholes, Fault Stick Diagrams, etc.

Hansreudi Maurer, lecture, Borehole Geophysics 2020 ETH Zürich.

Appendix A: Hydraulic Test data ST2

Test Interval Designation	Top Interval depth [m]	Bottom Interval depth [m]	Interval thickness	Suspect Fracture depth [m]	ST2 Wellhead Flow Rate [l/min]	Top Interval Flow Rate [l/min]	Bottom Interval Flow Rate [l/min]	Packer Interval Flow Rate [l/min]	MB1 Flow Rate [l/min]	Testing Date
F4	244.3	350.0	105.8		24.32	7.70	17.75			28/08/2020
F9	293.3	350.0	56.7		24.20	23.00	0.70			28/08/2020
T8	281.8	291.7	9.9	287		9.50	0.14	16.90		28/08/2020
T8	281.8	291.7	9.9		16.17	8.15		8.69	19.83	01/09/2020
T12	333.8	350.0	16.2	339.5		15.80	0.12			01/09/2020
T11a	324.8	334.6	9.9	330.5				0.0093		01/09/2020
F10a	310.0	319.9	9.9	318.5			0.46	0.00		01/09/2020
T10a	315.5	325.4	9.9	322.5		14.32		0.18		01/09/2020
T10a	315.5	325.4	9.9			14.17	0.30		16.81	02/09/2020
T9a	293.3	303.2	9.9	298.2		11.49	0.61	0.19		03/09/2020
T7	270.8	280.6	9.9	279.9	11.70	7.04	1.59	0.21		03/09/2020
T6a	255.9	265.8	9.9	259.8	19.15	7.33	5.95	0.45	21.46	03/09/2020
T5a	244.8	254.7	9.8	253.5	19.01	6.99	12.90	0.037	21.91	03.09.2020 - 04.09.2020
F6	287.4	350.0	62.6		18.49	9.82	5.73			04/09/2020
F6	287.3	350.0	62.7		18.12	9.82	5.28			04/09/2020
F6	287.2	350.0	62.8		18.24	8.35	6.42			04/09/2020
F6	287.1	350.0	62.9		18.30	7.71	6.76			04/09/2020
F6	286.8	350.0	63.2		18.95	7.65	6.69			04/09/2020
T4a	217.1	226.9	9.8	223.2			4.47	0.53	25.65	04/09/2020
T3a	210.4	220.3	9.8	213.4		4.10	12.76	1.24	29.33	04.09.2020 - 05.09.2020
F3	197.2	350.0	152.8		17.94	5.16	12.46			05/09/2020
F2a	185.8	195.6	9.8	194.5		4.88	11.22	0.05	18.77	05/09/2020
F1a	178.9	188.8	9.8	186.8	16.27	4.80	11.91	0.13	24.07	05/09/2020
T2a	168.1	177.9	9.8	174.8	15.84	0.35	9.75	4.25	23.03	05/09/2020
T1a	157.1	166.9	9.8	163	16.27	0.07	14.76	0.32		05/09/2020

Table 4- Flow rate data for ST2. Columns highlighted based on value, Green = larger vales, Red = smaller values (F. Christe, F. Serbeto and P. Meier, 2020).

Test Interval Designation	Top Packer depth [m]	Bottom Packer depth [m]	Suspect Fracture depth [m]	**Interval Transmissivity Estimate IARF-1 [m2/s] (11)**
T1	157.1	166.9	163	2.76E-08
T2	167.8	177.7	174.8	1.70E-07
F1	178.9	188.8	186.8	1.48E-08
F2a	185.8	195.6	194.5	2.98E-09
T3	210.4	220.3	213.4	1.66E-07
T4	217.1	226.9	223.2	4.14E-08
T5	244.8	254.7	253.5	4.10E-09
T6	255.9	265.8	259.8	2.93E-08
T7	270.8	280.6	279.9	2.55E-08
T8	281.8	291.7	287.5	**7.70E-07**
T9	293.3	303.2	298.2	-
T10	315.5	325.4	322.5	6.32E-09
T12	333.8	343.7	339.50	3.43E-09

Table 5- Interval Transmissivity flow rates derived using the Jacob Cooper method for ST2. Green = largest, Red = smallest. (F. Christe, F. Serbeto and P. Meier, 2020)

Appendix B: Hydraulic Test Data CB1

Test Interval Designation	Top Packer depth [m]	Bottom Packer depth [m]	Suspect Fracture depth [m]	Flow Rate [l/min] (1)		Transmisivity Estimate IARF-1 [m2/s] (11)
HT-1	137.0	145.7	143.8	0.80		2.21E-08
HT-2	180.6	189.3	181.7	1.70		4.51E-08
HT-3	184.0	192.7	186.3	2.10		1.30E-07
HT-4	192.3	201	198.3	0.70		3.23E-08
HT-5	203.0	211.7	208.4	0.70		1.53E-08
HT-6	211.0	219.7	213.8	0.90		1.95E-08
HT-7	225.3	234	227.2	0.00		-
HT-8	229.6	238.3	236.3	< 0.01		-
HT-9	239.3	248	243.3	2.00		3.15E-08
HT-10	249.0	257.7	250.5	< 0.01		-
HT-11	265.3	274	267.2	0.01		-
HT-12	275.0	283.7	277.6	9.00		2.38E-07

Table 6- Wellhead Flow rate and Transmissivity estimates for the CB1 hydraulic intervals. Green = largest, Red = smallest. (F. Christe, F. Serbeto and P. Meier, 2020)

Appendix C: Transmissivity and Fracture Zone comparisons

Connected Fault Name	ST2 Fault Zone thickness	Transmissivity ST2	CB1 Fault Zone thickness	Transmissivity CB1
11*	1.85	2.76E-08	1.2	2.21E-08
10*	1.5	2.98E-09	1	1.30E-07
9*	1.2	1.48E-08	1.5	4.51E-08
8*	1.2	4.14E-08	0.75	1.53E-08
5*	0.8	1.48E-08	0.6	4.51E-08
1*	0.6	7.70E-07	0.4	2.38E-07
6*	0.5	1.66E-07	0.7	3.23E-08
6*	0.15	4.14E-08	0.7	1.95E-08

Table 7- Comparisons of the Fault Zone thicknesses with Transmissivity values. Green = high values. Red= low values. (F. Christe, F. Serbeto and P. Meier, 2020)

Appendix D: Drilling Data and OTV log view

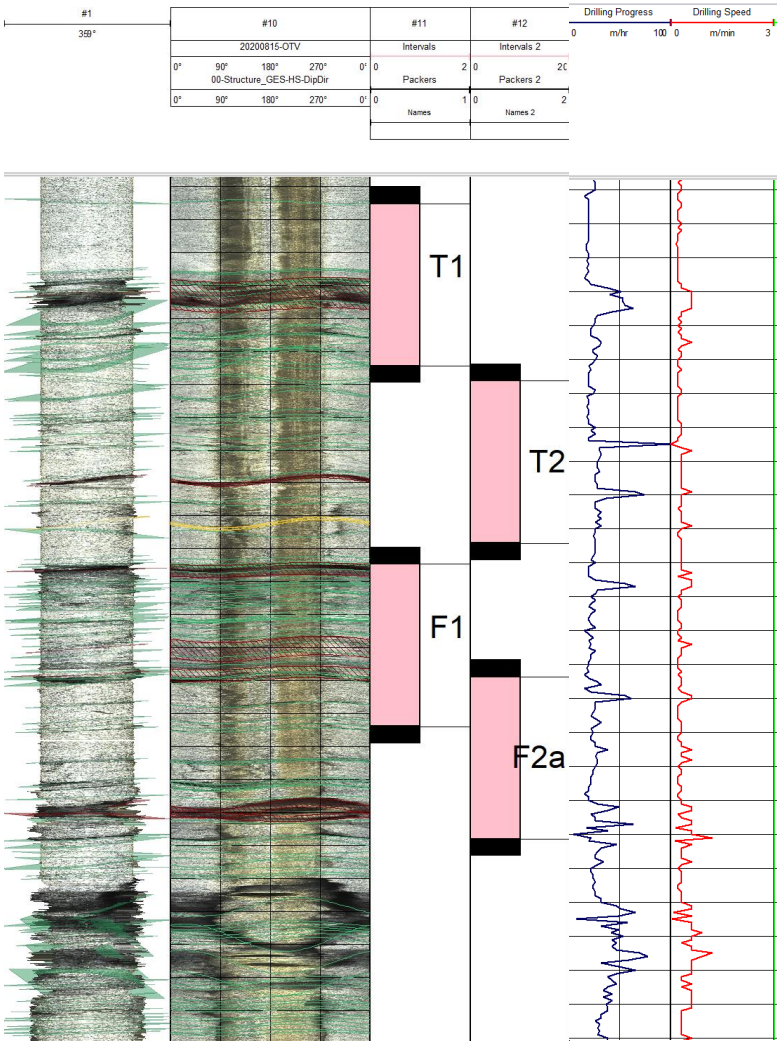

Figure 5- ST2 composite log showing the drilling progress and drilling speed [m/h] in relation to the OTV structures.

Appendix D- Drilling Data and OTV log view

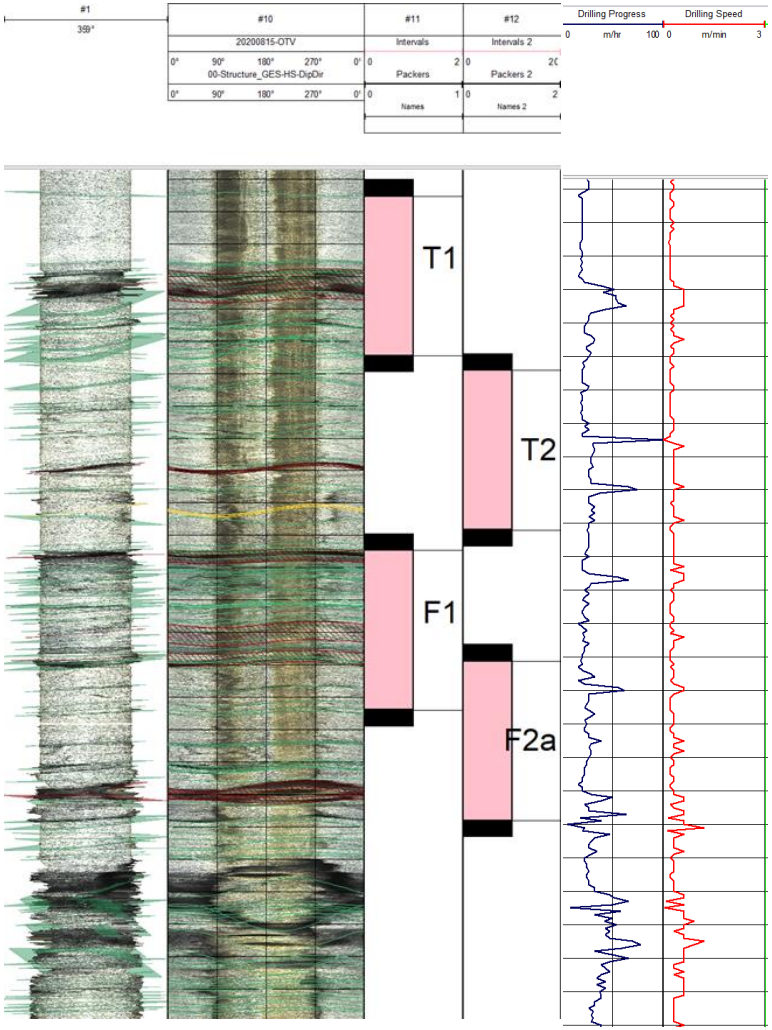

Figure 6- ST2 logs showing the Drilling progress and Drilling Speed [m/h] for the respective structures in the OTV log.

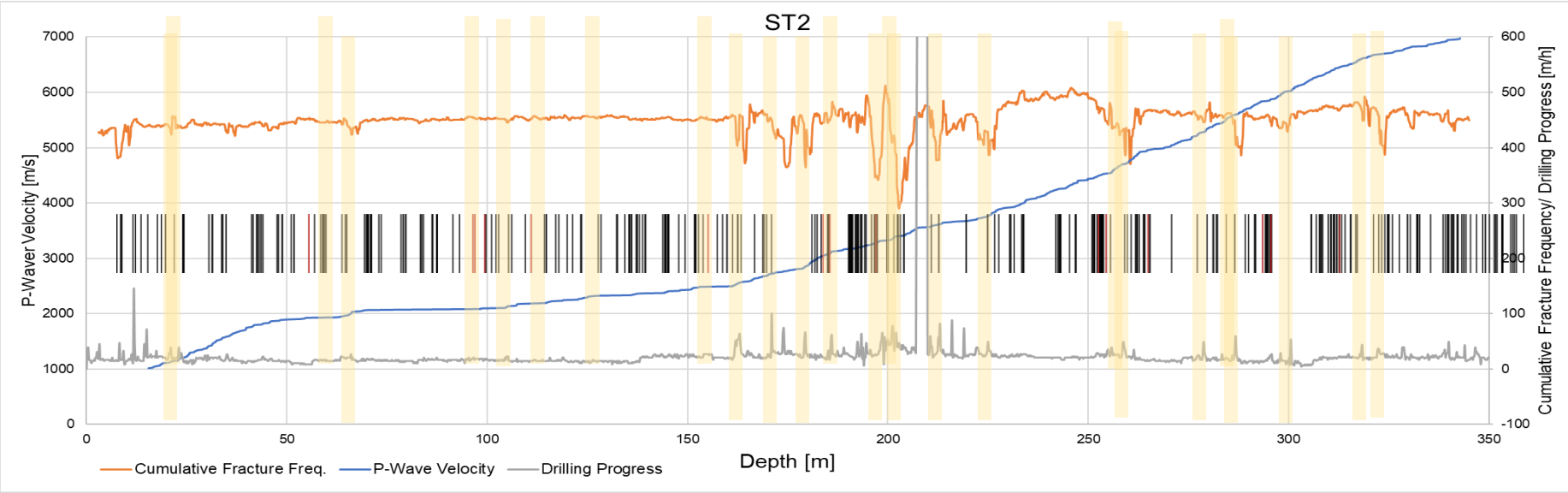

Figure 15- Graph of P -wave velocity, cumulative fracture frequency and Drilling progress: (upper) ST1 (lower) ST1. Structure stick diagrams are added to see the fracture densities better, the red sticks refer to the picked fault zones (R. Castilla, 2020